Oceanologia (2018) 60, 446—463

Available online at www.sciencedirect.com

ScienceDirect

journal homepage: www.journals.elsevier.com/oceanologia/

ORIGINAL RESEARCH ARTICLE

Spatiotemporal changes in the concentration and composition of suspended particulate matter in front of Hansbreen, a tidewater glacier in Svalbard

Mateusz Moskalik [a,*], Joanna Ćwiąkała [a], Witold Szczuciński [b], Aleksander Dominiczak [b], Oskar Głowacki [a], Kacper Wojtysiak [a], Piotr Zagórski [c]

[a] *Institute of Geophysics, Polish Academy of Sciences, Warszawa, Poland*
[b] *Institute of Geology, Adam Mickiewicz University in Poznań, Poznań, Poland*
[c] *Faculty of Earth Sciences and Spatial Management, Maria Curie-Skłodowska University, Lublin, Poland*

Received 31 July 2017; accepted 19 March 2018
Available online 5 April 2018

KEYWORDS
Seasonality;
Suspended particulate matter;
Particulate organic matter;
Tidewater glacier;
Fjord;
Svalbard

Summary Tidewater glaciers supply large amounts of suspended particulate matter (*SPM*) and freshwater to fjords and affect oceanographic, sedimentological and biological processes. Our understanding of these processes, is usually limited to the short summer season. Here, we present the results of a one-year-long monitoring of the spatial variability in *SPM* characteristics in a context of oceanographic and meteorological conditions of a glacial bay next to Hansbreen, a tidewater glacier in Hornsund (southern Spitsbergen). The observed range of *SPM* concentrations was similar to ranges measured in other sub-polar glaciated fjords, especially in Svalbard. The major source of SPM is the meltwater discharge from the glacier. The maximum water column-averaged *SPM* concentrations did not correlate with peaks in freshwater discharge and were observed at the beginning of the autumn season, when the fjord water transitioned from stratified to fully mixed. The observed spatiotemporal variations in the total *SPM*, particulate organic matter (*POM*) and particulate inorganic matter (*PIM*) are likely controlled by a combination of factors including freshwater supply, water stratification and circulation, bathymetry, the presence of sea ice, biological productivity and sediment resuspension. During the ablation season, the *SPM* maximum concentrations were located within the upper water layer, whereas

* Corresponding author at: Institute of Geophysics, Polish Academy of Sciences, Księcia Janusza 64, 01-452 Warszawa, Poland. Tel.: +48 226915883.
E-mail address: mmosk@igf.edu.pl (M. Moskalik).
Peer review under the responsibility of Institute of Oceanology of the Polish Academy of Sciences.

ELSEVIER Production and hosting by Elsevier

https://doi.org/10.1016/j.oceano.2018.03.001

during the winter and spring, the greatest amounts of *SPM* were concentrated in deeper part. Thus, typical remote sensing-based studies that focus on *SPM* distributions may not reflect the real *SPM* levels. *POM* and *PIM* concentrations were correlated with each other, during most of the time suggesting that they may have a common source.

1. Introduction

Glaciers are one of the most sensitive indicators of ongoing climate changes that have commonly resulted in their recent very rapid retreat since the end of the Little Ice Age (e.g., Carr et al., 2017; Radić and Hock, 2011; Solomina et al., 2016). Due to the retreat of marine-terminating tidewater glaciers, at a rate of several tens of metres per year, as in Svalbard (e.g., Błaszczyk et al., 2013), or several hundreds of metres per year, as in Alaska (e.g., Molnia, 2007), new glacial bays have formed and host immature coastal ecosystems. Melting glaciers affect coastal waters in many ways, the most important of which is the delivery of freshwater and suspended particulate matter (*SPM*), which is often called suspended sediment. They are among the key driving factors for coastal glaciomarine ecosystems, as well as oceanographic and sedimentary regimes (e.g., Bennett and Glasser, 2009; Chauche et al., 2014; Motyka et al., 2003; Szczuciński and Zajączkowski, 2012). Their influence can also extend far beyond the coastal zone into the open ocean and affect larger scale circulation and biological processes. For example, *SPM*-rich glacial meltwater can provide critical limiting micronutrients (e.g., Fe) to the ocean and thereby influence its primary production (e.g., Bhatia et al., 2013; Markussen et al., 2016).

Many of the existing records of sediment accumulation rates in fjords suggest that climate warming has enhanced sediment production and export to the fjords (Boldt et al., 2013; Koppes and Hallet, 2002; Szczuciński et al., 2009; Zajączkowski et al., 2004). In addition, the combination of historical data and modelling experiments suggests that present-day sediment fluxes to the polar zone of the coastal ocean have increased. For instance, the suspended sediment supply from Greenland to the ocean is currently approximately 56% higher than it was during the 1961–1990 period (Overeem et al., 2017). Moreover, one may expect that the seasonality of *SPM* delivery, distribution and sedimentation processes will also change. However, this issue is still open to research because present-day seasonal changes in *SPM* distributions are poorly known.

SPM is mainly delivered to fjords by ice-contact processes, including meltwater discharge, rafting by icebergs and sea ice, riverine inputs and exchanges with external water masses (Syvitski, 1989; Winters and Syvitski, 1992). The general model of *SPM* delivery shows the driving role of freshwater and sediment-laden outflows from tidewater glaciers, which, due to density differences, form surface brackish water plumes covering most of the glacial bays during the summer season (Syvitski, 1989). However, a growing number of observations, indicate that other factors are also significant. For example, a study on a large dataset from Greenland found that the delivery of *SPM* is likely mainly a function of the regional glacial dynamics and the resulting intensity of erosion, not freshwater flux (Overeem et al., 2017). Furthermore, oceanographic circulation is important not only in terms of the sediment transport and circulation patterns in glacial bays but also as a driving factor of tidewater glacier stability (e.g., Straneo and Heimbach, 2013). Because field observations on seasonal cycles are sparse, the driving forces that control the *SPM* input and distribution in fjords are still subject to ongoing debate.

The fjords of Svalbard are particularly suitable for studies on climate warming impacts on the supply and fate of *SPM* since they are affected by the northward flowing West Spitsbergen Current (WSC) that transports warm Atlantic Water (AW), resulting in accelerated warming (e.g., Cisek et al., 2017; Osuch and Wawrzyniak, 2016; Promińska et al., 2017). Moreover, these fjords are among the best studied subpolar fjords in the world, and many supplementary data are available (e.g., Drewnik et al., 2016; Forwick et al., 2010; Svendsen et al., 2002). The *SPM* concentrations in the fjords of Svalbard are commonly documented during the summer season in central parts of fjords (e.g., Sagan and Darecki, 2018; Svendsen et al., 2002), in meltwater river-fed bays (e.g., Dowdeswell and Cromack, 1991; Zajączkowski and Włodarska-Kowalczuk, 2007) and in the glacial bays near tidewater glaciers (e.g., Elverhøi et al., 1983; Görlich et al., 1987; Schildt et al., 2017; Szczuciński and Zajączkowski, 2012; Trusel et al., 2010; Urbanski et al., 2017; Zajączkowski, 2002, 2008).

However, observations on the seasonal *SPM* concentration changes and their major controlling factors in the fronts of tidewater glaciers in Spitsbergen are very limited. Szczuciński and Zajączkowski (2012) studied sedimentary processes in the summer and autumn in Adolfbukta next to the calving front of Nordenskiöldbreen. These authors found that in the autumn, the vertical particulate matter fluxes (sedimentation) decrease much more than the *SPM* concentrations and that residence time of the *SPM* in the water increases likely due to less effective flocculation. These authors also suggested a list of factors that affect the sedimentation of *SPM*, such as the positions of freshwater inlets (surface/subsurface), meltwater discharge, *SPM* concentrations in the meltwater, local wind damming effects, tides and resuspension. Moreover, studies conducted in glacier-distal settings revealed that phytoplankton blooms are important factors in the increase of *SPM* concentrations in the spring (Pawłowska et al., 2011; Węsławski et al., 1988).

The goal of the paper is to present a unique time series of the seasonal changes of the *SPM* delivery, distribution and composition in a glacial bay next to the calving front of Hansbreen in Hornsund. This paper presents a

complementary dataset, including supporting meteorological and oceanographic monitoring data, for the period from May 2015 to June 2016. The obtained data are used to identify major *SPM* sources and driving processes responsible for *SPM* spatial distribution and composition during various seasons.

2. Study area

Hornsund is an approximately 34 km long fjord in the southwest part of Spitsbergen. Glaciers cover approximately 60% of its catchment (Błaszczyk et al., 2009, 2013). The most frequently studied glacier in Hornsund is Hansbreen, a polythermal tidewater glacier that ends with a 1.5 km wide calving cliff in Hansbukta (Hans Bay), which is almost 80 m deep. The bay covers an area of 6 km^2, and its outer region, with a maximum depth of less than 25 m, is shallower than its innermost region (Ćwiąkała et al., 2018) (Fig. 1). The bay was formed during the last century due to glacier retreat; presently, the glacier retreats approximately 40 m year^{-1} (Błaszczyk et al., 2013). The Hansbreen area is 56 km^2, and its mean ice thickness is approximately 170 m (Błaszczyk et al., 2013; Grabiec et al., 2012). The bedrock beneath the glacier is composed of various types of low to intermediate grades of metamorphic rocks including schists, gneisses, amphibolites, marbles and quartzites (Birkenmajer, 1990). The meltwater is delivered from Hansbreen to the bay mainly through subglacial tunnels that enter the bay from the central and eastern parts of the glacier cliff (Pälli et al., 2003).

The WSC and East Spitsbergen Current (ESC) influence the oceanographic conditions of Hornsund and make its climate

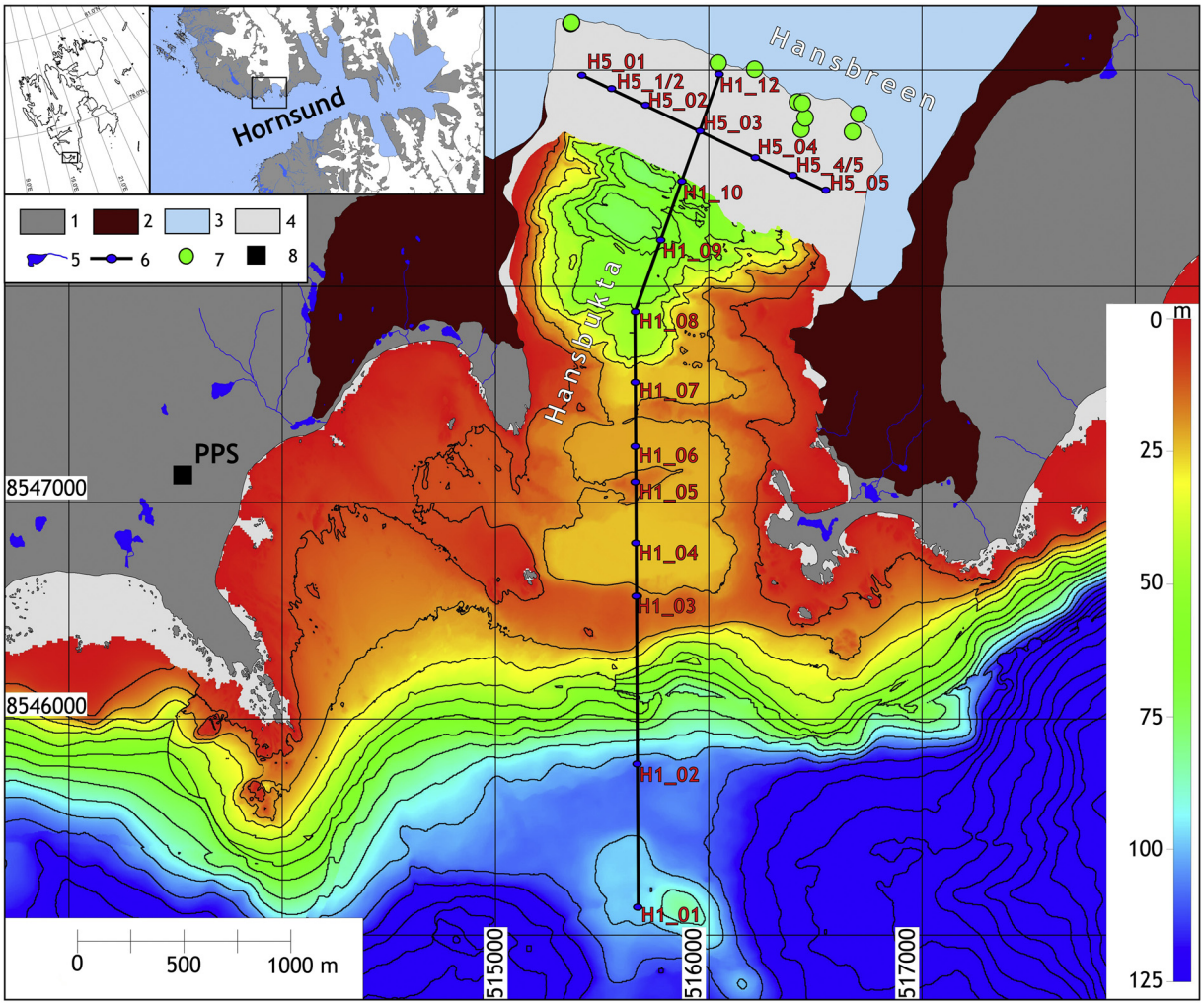

Figure 1 Study area: Hansbukta with transects and monitoring stations marked. Legend: 1 — land, 2 — moraines on land, 3 — glaciers, 4 — marine areas with no bathymetry data, 5 — lakes and rivers, 6 — ADCP transects and monitoring stations, 7 — outflows from the glaciers (based on satellite images collected between the 6th of June and 1st of October 2015), 8 — the meteorological station in the Polish Polar Station (PPS). The inset maps show the location of the study area within the Hornsund Fjord and the location of Hornsund within the Svalbard archipelago.
Sources: Shoreline, lakes, rivers, glaciers and moraines are based on the Norsk Polar Institute data (http://geodata.npolar.no/) (updated for the Hansbreen position in 2015), bathymetric data are from The Norwegian Hydrographic Service (the permit for data use was issued by the Institute of Geophysics, Polish Academy of Sciences no. 13/G722) with isobaths every 10 metres.

mild and maritime (Marsz and Styszyńska, 2013; Osuch and Wawrzyniak, 2016). The mean annual air temperature from 1979 to 2014 was approximately −4.0°C, with the highest temperature recorded in July and the coldest in March. The mean annual precipitation during the same period was approximately 450 mm, with the highest amounts during the late summer and autumn seasons and the lowest during spring (Osuch and Wawrzyniak, 2016). Approximately 60% of the mean total annual precipitation in the region falls as snow or sleet (Łupikasza, 2013). On average, the snow cover occurs approximately 240 days of the year, with maximum mean snow depths in April. However, the snow depths and durations vary strongly from year to year (Kępski et al., 2017).

The fjord water masses are generally stratified during the ablation season, then they are subjected to mixing in the autumn and winter. Moreover they are affected by the inflow of water masses from the Greenland Sea, as documented in previous oceanographic studies (e.g., Drewnik et al., 2016; Görlich, 1986; Promińska et al., 2017; Węsławski et al., 1991, 1995). Consequently, six types of water masses were distinguished according to the classification system for fjords of Svalbard. The AW and Transformed Atlantic Water (TAW) masses enter the fjord from the shelf. The AW comes from the WSC, and its temperature and salinity are higher than 3°C and 34.9 PSU respectively. The TAW is a mix of AW and Arctic-type Water (ArW) from the ESC and has a temperature between 1°C and 3°C and a salinity higher than 34.7 PSU. The third type of water mass is Surface Water (SW), which is the uppermost layer formed from the glacial melt water. SW is common from late spring to autumn and has a water temperature higher than 1°C and a salinity lower than 34.7 PSU. Mixing of the SW and AW or TAW forms Intermediate Water (IW), with a temperature higher than 1°C and a salinity between 34 and 34.7 PSU. Cooling during the winter generates Local Water (LW), with a temperature lower than 1°C and Winter Cooled Water (WCW) with a temperature lower than −0.5°C and salinity higher than 34.4 PSU (Nilsen et al., 2008). The circulation in the fjord is enhanced by the Coriolis force (Jakacki et al., 2017; Pawłowska et al., 2017) and the tides with mean spring tidal range of over 1 m. Lately, the fast ice cover in Hornsund usually covers more than 40% of the fjord and last for approximately 45 days per year (Muckenhuber et al., 2016).

3. Material and methods

3.1. Meteorology

The meteorological data, including air temperature (Fig. 2A) and precipitation (Fig. 2B), from the period from May 2015 to June 2016 were obtained from the Polish Polar Station Hornsund (PPS), which is located 2 km west from Hansbukta. The daily mean air temperatures were smoothed by a robust local regression using a weighted least squares method and second degree polynomial model with a 45-day duration (LOESS model implemented in MATLAB software).

3.2. Oceanography

The water temperature and salinity values were measured using a Valeport miniCTD probe (CTD) during 22 surveys at 18 monitoring stations along 2 transects (Fig. 1). Due to equipment failure, CTD measurements were not made from December 2015 to March 2016. Most of the figures in this paper are based on data from monitoring station H1_09 (Fig. 2C and D), which is considered a representative station because it is located in the deepest central part of the bay, almost 1000 m from the glacier cliff (Fig. 1). At that station, the freshwater from all the meltwater outflows is mixed. The temperature and salinity data from that station were smoothed by a robust local regression using a weighted least squares method and second degree polynomial model for 10 m depth sections (LOESS model implemented in MATLAB software) and interpolated over time using a cubic Hermite spline (method implemented in MATLAB software) to obtain the seasonal fluctuations in the water properties (Fig. 3A and C).

To obtain information about seasonal water stratification changes, the water temperature standard deviation (σ_T) for the depth profile at station H1_09 was calculated from the measured and interpolated data (Fig. 3B). Higher values of σ_T imply greater temperature ranges in the depth profile and, consequently, the development of stratification. Values of σ_T close to zero indicate no stratification in the water column.

To determine the input by the meltwater discharge from the glacier, the freshwater fraction (*FWF*) was calculated for the interpolated and measured salinity (Fig. 3D). Guided by Ketchum (1950) and Nut and Coachman (1956), the *FWF* was calculated using the equation:

$$FWF = \frac{(S_0 - S)}{S_0} \cdot 100\%, \quad (1)$$

where S_0 = 34.92 PSU, which was the highest measured salinity (from H1_01, which is the point nearest to the mouth of the Hornsund Fjord), and S is the average salinity in the water column at station H1_09.

To identify the circulation pattern in the bay, a Teledyne RD Instruments Workhorse Sentinel 600 kHz Acoustic Doppler Current Profiler (ADCP) was used twice during the summer, on the 13th of July, and the 1st of September 2015, along transects perpendicular and parallel to Hansbreen cliff (Fig. 1). The velocity (Fig. 4B, E, H, K) and the direction (Fig. 4A, D, G, J) of the flow were directly measured by the ADCP.

The positions of meltwater outflows from Hansbreen were marked on satellite images collected by Landsat 8 (images from U.S. Geological Survey Department of Interior for the years 2015 and 2016) based on the method outlined by Dowdeswell et al. (2015), in order to compare them with water circulation and *SPM* concentration data.

Information about the sea ice conditions in Hansbukta during the measurement period were based on the observations that were made by the authors and PPS staff (Fig. 2C).

3.3. Suspended particulate matter

Spatial and temporal changes in *SPM* were obtained from the ADCP measurements and filtered water samples. The echo strength (in counts) measured by the ADCP provided insight into the acoustic intensity Int_{ADCP} (in dB):

$$Int_{ADCP} = 20 \cdot \log_{10}(R) + 2 \cdot \alpha \cdot R + K_C \cdot E + C_K, \quad (2)$$

where R is the range along the beam (in m), α is the attenuation coefficient due to water absorption (in dB m^{-1}),

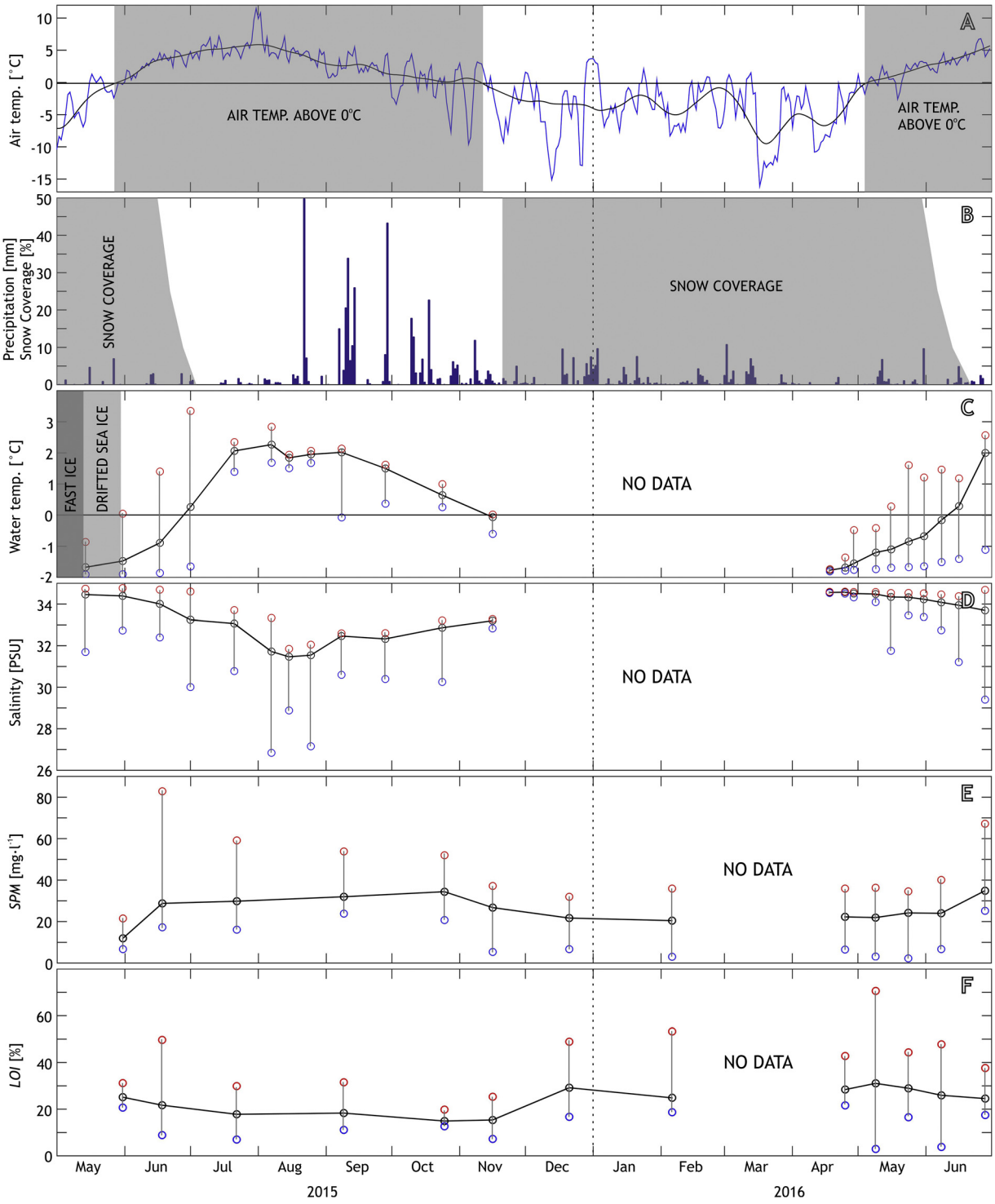

Figure 2 Annual course of the meteorological conditions at the Polish Polar Station (PPS), including oceanographic conditions from station H1_09, and suspended particulate matter (*SPM*) with loss on ignition (*LOI*) data from all the sampling stations (see Fig. 1 for site locations). (A) Daily mean (blue line) and smoothed (black line) air temperature; (B) daily precipitation and snow coverage (based on Kępski et al., 2017); (C) mean (black circles linked by black line), minimum (blue circles) and maximum (red circles) water temperatures and sea ice conditions; (D) mean (black circles linked by black line), minimum (blue circles) and maximum (red circles) water salinity; (E) mean (black circles linked by black line), minimum (blue circles) and maximum (red circles) *SPM* concentrations; (F) mean (black circles linked by black line), minimum (blue circles) and maximum (red circles) *LOI* in *SPM*. (For interpretation of the references to color in this figure legend, the reader is referred to the web version of this article.)

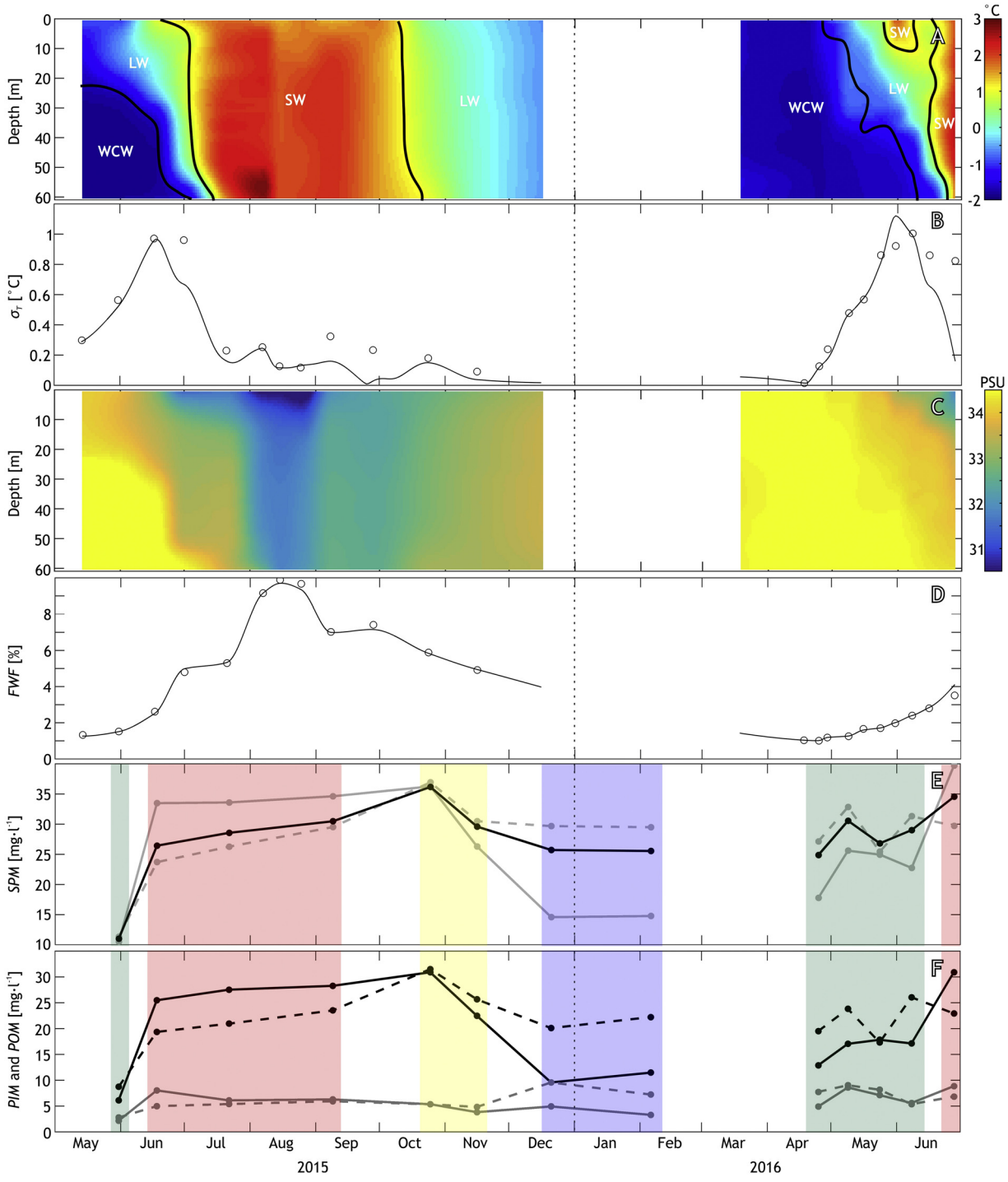

Figure 3 Annual changes in the oceanographic conditions of station H1_09 (for station location see Fig. 1) and mean interpolated suspended particle matter (*SPM*) concentration and composition data. (A) Interpolated water temperature depth profile changes over time. The abbreviations refer to water mass types. WCW — winter-cooled water, LW — local water, and SW — surface water (see text for details); (B) standard deviations of water temperature (σ_T) from interpolated (black line) and measured (black circles) values; (C) interpolated water salinity depth profile changes over time; (D) the freshwater fraction (*FWF*) calculated from interpolated (black line) and measured (black circles) values; (E) the mean concentration of *SPM* from interpolated data over the total water column (black line), its surface concentration (grey line) and deeper subsurface concentration (dashed grey line). The surface part of the water column refers to the layer from the surface to a depth of 10 m, and deep water refers to the layer from 20 to 50 m below surface; (F) average concentrations of the interpolated particulate inorganic matter (*PIM* — black lines) and particulate organic matter (*POM* — grey lines) within the surface (solid lines) and deeper subsurface (dashed lines) parts of water. The time intervals coloured on (E) and (F) represent measurements assigned to the spring (green), summer (red), autumn (yellow), and winter (blue) seasons. (For interpretation of the references to color in this figure legend, the reader is referred to the web version of this article.)

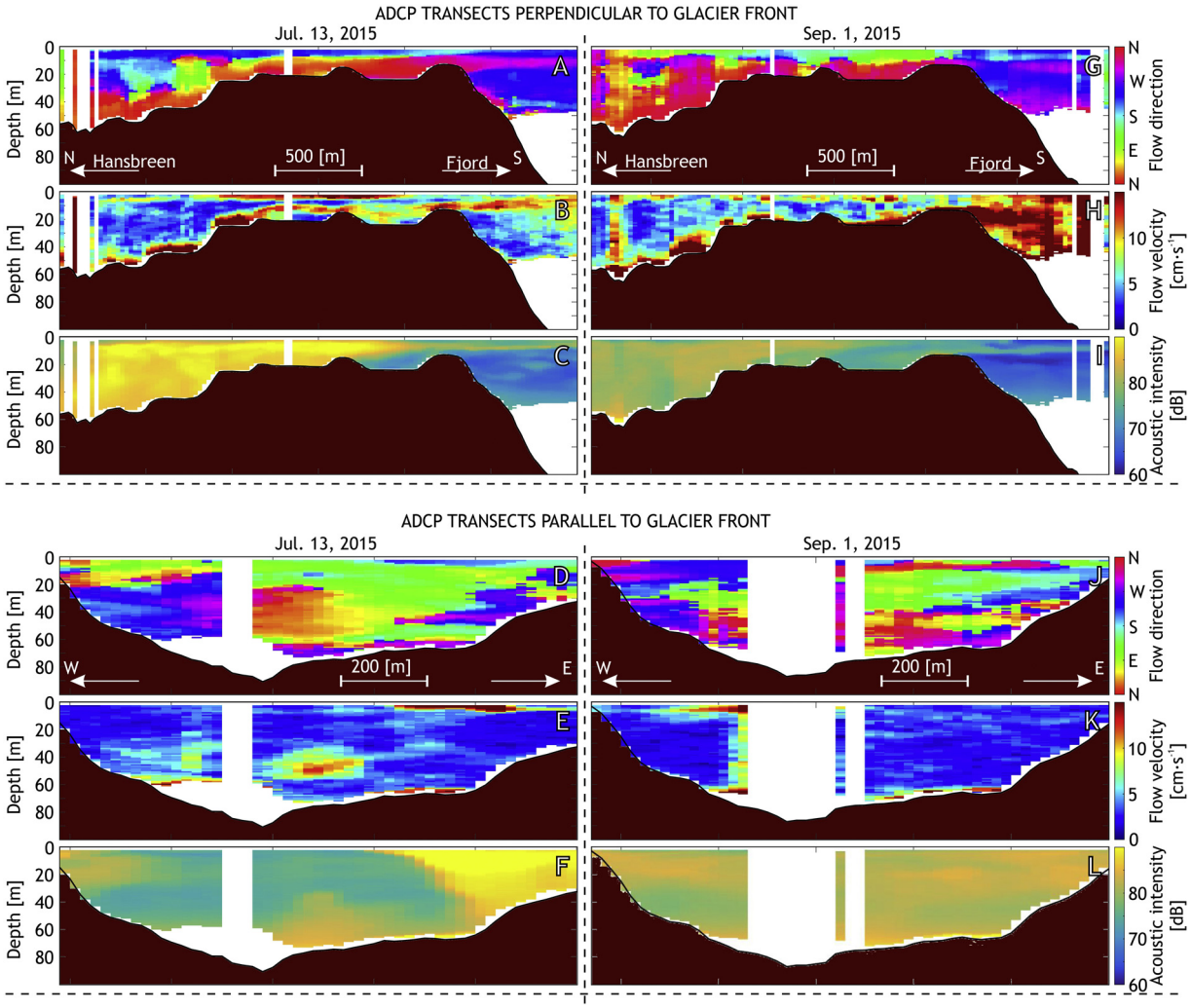

Figure 4 Acoustic Doppler Current Profiler (ADCP) measurements made on the 13th of July 2015 (A–F) and 1st of September 2015 (G–L) on transects perpendicular (A–C, G–I) and parallel (D–F, J–L) to the glacier front (for locations see Fig. 1). A, D, G and J present the flow directions, B, E, H and K show the flow velocity, and C, F, I and L represent the acoustic intensity.

E is the echo strength measured by the ADCP (in counts), and K_C (in dB counts^{-1}) and C_K (in dB) are constants. The values of the constants are calculated during the calibration procedure. The K_C value ranges from 0.35 to 0.55 dB counts^{-1} and is typically 0.45 dB counts^{-1} (Deines, 1999; Kim and Voulgaris, 2003). Using the latter value a modified acoustic intensity (*Int*) may be calculated from:

$$Int = Int_{ADCP} - C_K = 20 \cdot \log_{10}(R) + 2 \cdot \alpha \cdot R + 0.45 \cdot E, \quad (4)$$

Int is related to *SPM* (concentration) (Deines, 1999; Kim and Voulgaris, 2003):

$$10 \cdot \log_{10}(SPM) = Int_{ADCP} \quad (5)$$

and based on Eqs. (4) and (5) the *SPM* (concentration) is expressed as:

$$SPM = 10^{0.1 \cdot C_K} \cdot 10^{0.1 \cdot Int}. \quad (6)$$

In this study, no calibration procedure was performed, so only *Int* was calculated (Fig. 4C, F, I, L).

Water samples were taken 13 times at regular intervals between the 31st of May 2015 and the 28th of June 2016, except of March 2015, using a Hydrobios Free Flow 1l Niskin Bottle at several water depths at the monitoring stations (Fig. 1). The samples (approximately 1 l each) were filtered through Whatman GF/F 0.7 μm filters that had been previously dried for 2 h at 200°C and weighed. There were no animals or plant fragments visible on the filters. After filtering, the filters were rinsed with fresh water and were dried for 24 h at 40°C and weighed again to calculate the *SPM* (Appendix 1, Fig. 2E). Subsequently, all filters were heated at 550°C for 3 h to calculate the loss on ignition (*LOI*), according to the Heiri et al. (2001) equation:

$$LOI = \frac{DW - DW_{550}}{DW} \cdot 100\%, \quad (7)$$

where *DW* is the dry weight of the sediments before heating and DW_{550} is the dry weight of the sediments after heating (Appendix 2, Fig. 2F). With the total *SPM* concentration and *LOI* values, particulate organic matter (*POM*) and particulate inorganic matter (*PIM*) concentrations were calculated:

$$\begin{aligned} POM &= SPM \cdot LOI \\ PIM &= SPM \cdot (1 - LOI) \end{aligned}. \quad (8)$$

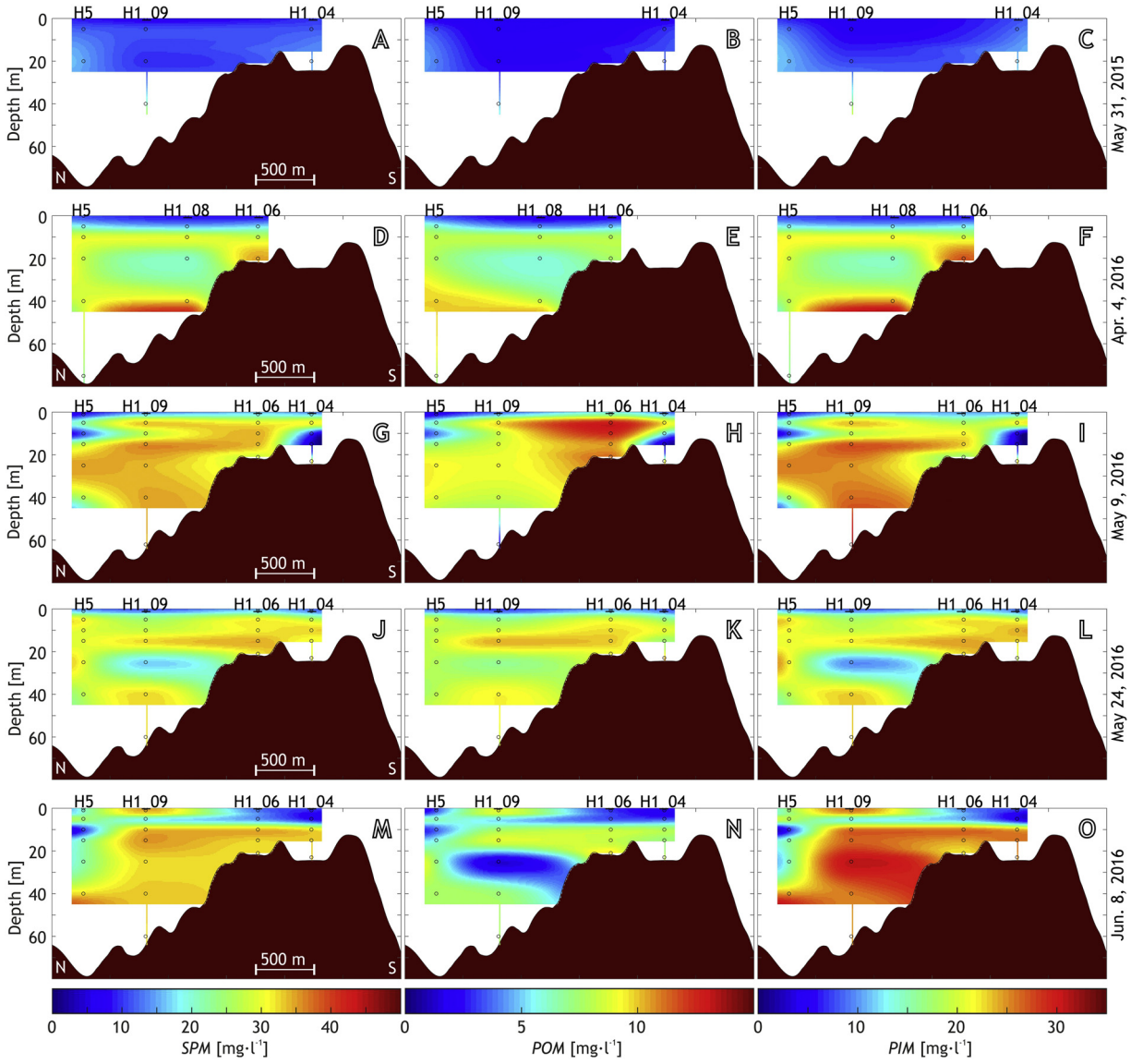

Figure 5 Interpolated distributions of suspended particulate matter (*SPM*) (A, D, G, J, M), particulate organic matter (*POM*) (B, E, H, K, N), and particulate inorganic matter (*PIM*) (C, F, I, L, O), during the spring season in Hansbukta. The interpolations are based on data from measurements taken on the 31st of May 2015 (A, B, C), 25th of April 2016 (D, E, F), 9th of May 2016 (G, H, I), 24th of May 2016 (J, K, L) and 8th of June 2016 (M, N, O). For the location of monitoring stations see Fig. 1.

To determine the spatial distribution of *SPM*, *POM* and *PIM*, the calculated data were interpolated using a cubic Hermite spline (a method implemented with MATLAB software) for the depth profile and between the profiles (Figs. 5–7). In the interpolated profiles perpendicular to the glacier cliff (Figs. 5–7), the data presented for station H5_03 (the closest station to the glacier cliff) are the average values from all the stations along a transect parallel to the glacier cliff. All the interpolated *SPM*, *PIM*, and *POM* data were used to represent the annual variability of the inner part of Hansbukta, up to 2000 m from the glacier. The data were averaged for two water layers: the surface (0–10 m depth) and deeper layer (20–50 m depth) (Fig. 3E and F) and analysed for the particular calendar seasons. Accordingly, the relationship of *POM* to *PIM* (Fig. 8A) and the *LOI* distributions (Fig. 8B–E) were analysed. The correlation coefficient and regression analysis using robust regression (each implemented within MATLAB software) were calculated for the *PIM* and *POM* values in the particular seasons (Fig. 8A, Table 1).

4. Results

4.1. Meteorological conditions

The daily mean air temperatures, precipitation and snow coverage during the study period (2015–2016) are presented in Fig. 2A and B. The air temperature was the highest (11.5°C) at the end of July and beginning of August 2015. The lowest daily mean air temperatures (down to −16.1°C) occurred in March 2016. The ablation season, defined as the period with positive air temperatures, lasted from the end of May 2015 to

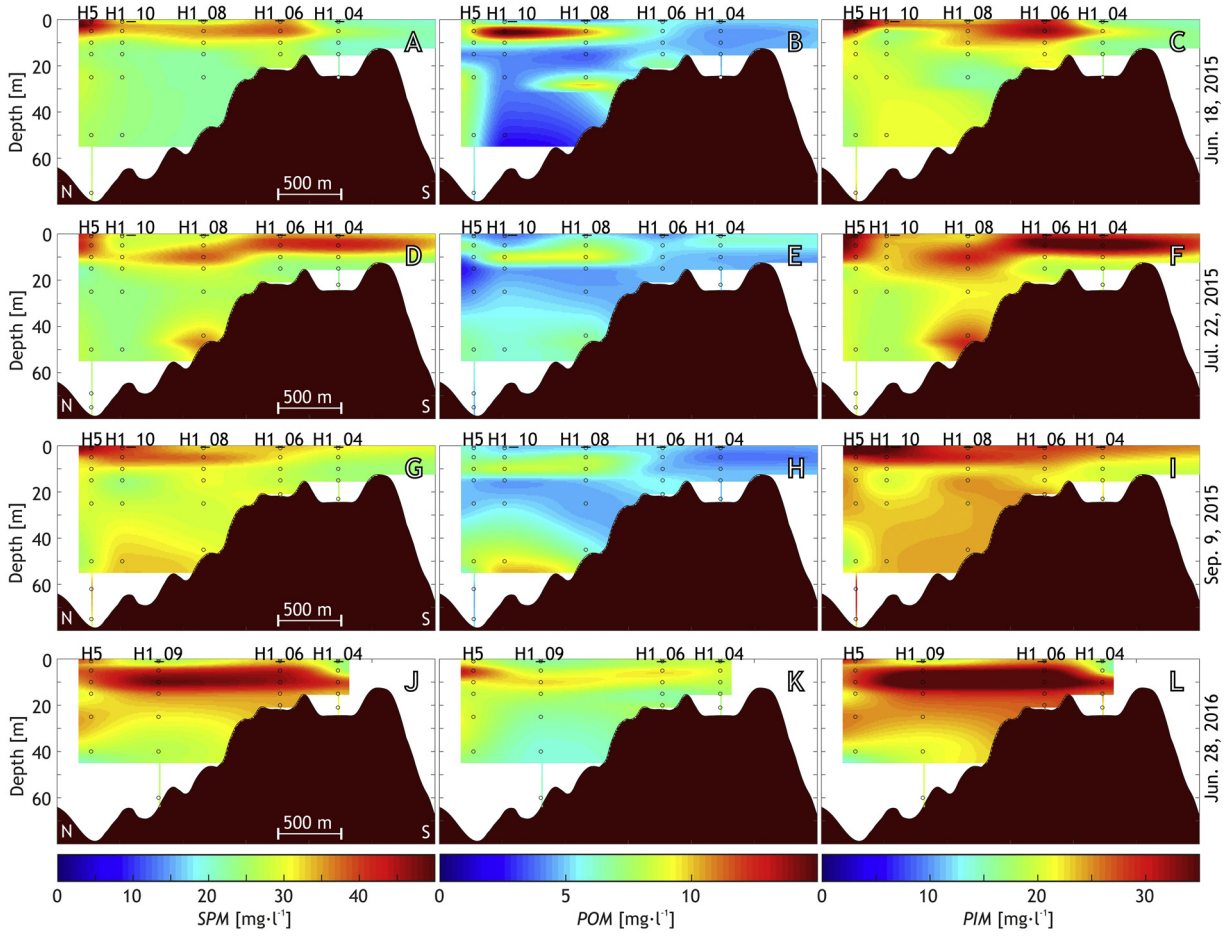

Figure 6 Interpolated distributions of suspended particulate matter (*SPM*) (A, D, G, J), particulate organic matter (*POM*) (B, E, H, K), and particulate inorganic matter (*PIM*) (C, F, I, L) during the summer season in Hansbukta. The interpolations are based on data taken on the 18th of June 2015 (A, B, C), 22nd of July 2015 (D, E, F), 9th of September 2015 (G, H, I), and 28th of June 2016 (J, K, L). For the location of monitoring stations see Fig. 1.

the middle of October 2015 and from the beginning of May 2016 to the end of the study period. However, during the winter, the daily average temperatures were above 0°C several times, particularly at the end of December and the beginning of January (Fig. 2A). Average daily air temperatures were close to 0°C during the second half of October and first half of November. The daily precipitation was low until the middle of August 2015, then precipitation values increased significantly and slowly decreased in autumn 2015 (Fig. 2B). In 2015, the snow coverage percentage was less than 50% in the middle of June and completely disappeared from coastal zone during the beginning of July. The snow coverage pattern in 2016 was similar, but the snow melting occurred about half a month earlier (Fig. 2B).

4.2. Oceanography

The oceanographic conditions revealed clear seasonal variations. The water temperature measured at station H1_09 ranged from −1.8°C during winter and early spring to more than 2°C at the end of July and beginning of August 2015 (Figs. 2C and 3A). The seasonality of the mean water temperature was characterised by a rapid increase from late spring to early summer, small fluctuations during summer and a gradual decrease during autumn. The water temperature increase during the spring/summer transition occurred about one month earlier in 2016 than in 2015 (Figs. 2C and 3A).

Water salinity ranged from less than 30 to almost 35 PSU (Figs. 2D and 3C). The highest salinity was measured during the early spring (May 2015, April and May 2016) and the lowest was measured during the summer (August 2015).

During the study period, three types of water masses were observed in the inner part of Hansbukta. In the spring, the WCW dominated (in 2015, it dominated below a 25 m depth, and in 2016 was present in complete water column). The dominant water mass became LW by the end of June in 2015 and by the middle of June in 2016. Then, in the span of a few days the LW mass was replaced with SW. The latter completely filled the inner part of Hansbukta during the summer of 2015, and it was replaced by LW in the autumn (mid-October 2015). The late autumn/winter period, during which WCW became the dominant water mass, was not documented due to a gap in the measurements. The periods of WCW transformation into LW and then into SW coincided with periods of distinct water stratification (Fig. 3A and C) with maximum σ_T values in June 2015, as well as at the end of May and beginning of June 2016 (Fig. 3B). During the summer (from mid-July to October 2015), stratification was less

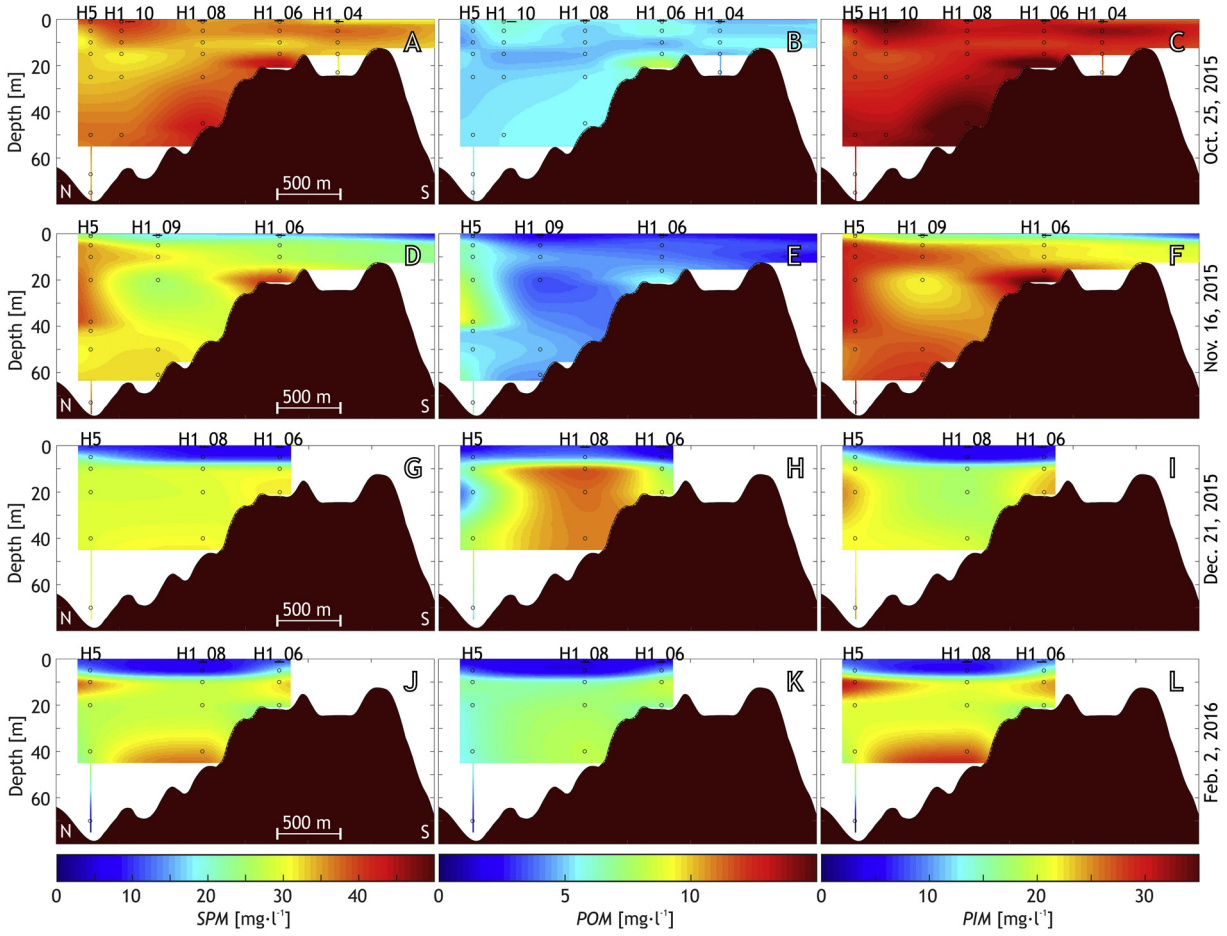

Figure 7 Interpolated distributions of suspended particulate matter (*SPM*) (A, D, G, J), particulate organic matter (*POM*) (B, E, H, K), and particulate inorganic matter (*PIM*) (C, F, I, L) during the autumn (A to F) and winter (G to L) seasons in Hansbukta. The interpolations are based on data taken on the 25th of October 2015 (A, B, C), 16th of November 2015 (D, E, F), 21st of December 2015 (G, H, I), and 6th of February 2016 (J, K, L). For the location of monitoring stations see Fig. 1.

pronounced and was restricted to the surface water layers. During the late autumn of 2015 and the early spring of 2016, the waters were well mixed (Fig. 3A–C).

The calculated *FWF* ranged from nearly 1% in spring 2015 and 2016 to almost 10% in summer, with a maximum in August 2015 (Fig. 3D). A rapid increase in the *FWF* was observed from the late spring (beginning of June) to the middle of the summer (beginning of August) 2015. The *FWF* slowly decreased in the autumn. During the spring of 2016, the increase in *FWF* was slower and started earlier than in the spring of 2015 (Fig. 3D).

The ADCP data from the mid-July, revealed two main flow directions in the inner part of Hansbukta (Fig. 4A, B, D, E). Surface flux, with a velocity between 10 and 15 cm s^{-1}, moved from the NE (east part of ice cliff) to SW (into the fjord), while near-bottom and mid-water depth flux, faster than 15 cm s^{-1}, had the opposite direction. In early September the fluxes were weaker and originated mainly from the western part of glacier cliff (Fig. 4G, H, J, K). The high flow velocity was observed in subsurface water and near the bottom, where current velocities along the bay were over 15 cm s^{-1} (Fig. 4A, B, D, E).

Fast ice was observed inside Hansbukta until the middle of May 2015. After this period, the bay and almost entire Hornsund fjord was covered by drifting sea ice until the end of May 2015. Almost no sea ice was observed during the 2016 season (Fig. 2C).

4.3. Suspended particulate matter

Information on the *SPM* distribution was obtained from satellite images and ADCP surveys for the mid- and late summer and from water sampling throughout the study period. The satellite images revealed the location of major freshwater sediment-laden subglacial outflows from the tide-water glacier cliff. The outflows were observed in the images from the 6th and 31st of June; 8th, 15th, and 17th of September; and the 1st of October 2015 as *SPM*-rich surface water plumes. In the case of the other available images, the weather was cloudy or outflows were not identified. The most prominent outflow was from the eastern part of the Hansbreen cliff, and it was seen in all the described satellite images. Moreover, a number of images contain emerging plumes from outflows located in the western (the 6th and 31st of June, the 15th and 17th of September and the 1st of October 2015) and central (the 15th of September and 1st of October 2015) parts of the glacier cliff (Fig. 1).

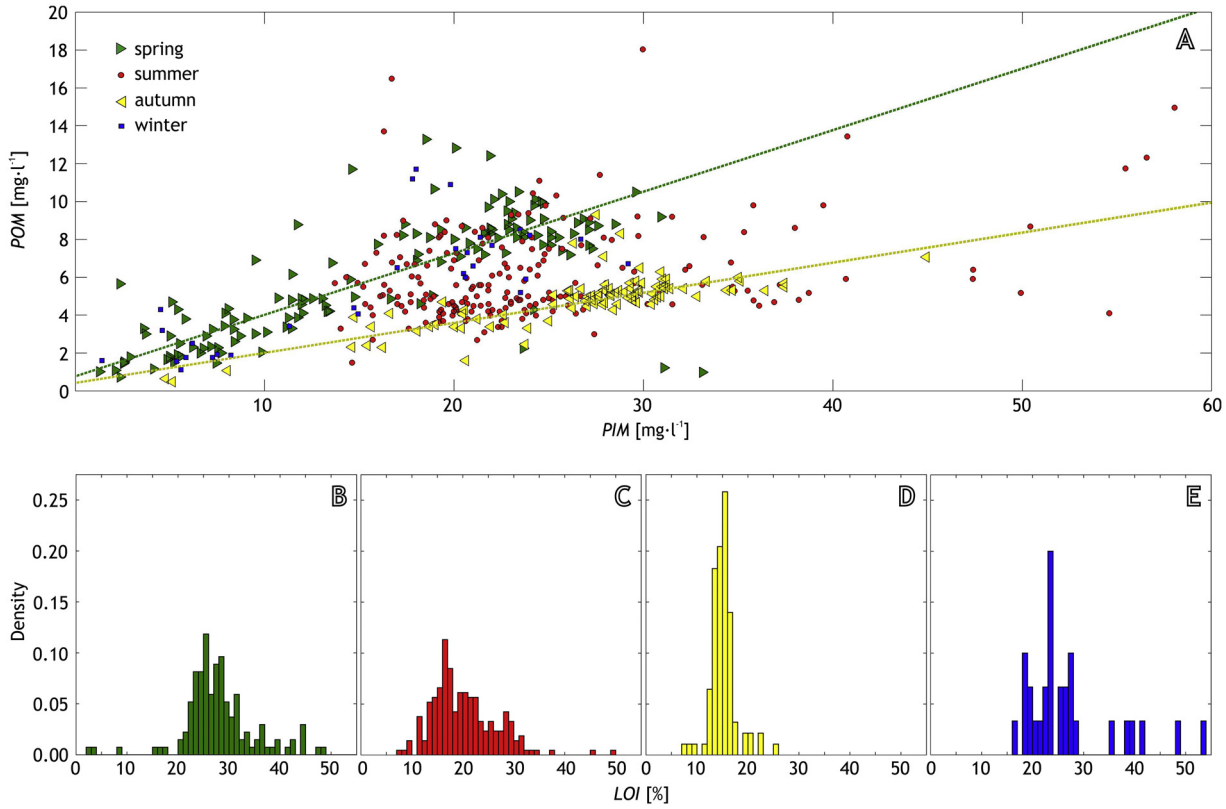

Figure 8 Changes in the composition of suspended particulate matter (*SPM*) over time. (A) Scatter plot of particulate inorganic matter (*PIM*) and particulate organic matter (*POM*) concentrations with linear regressions for the spring (green dotted line) and autumn seasons (yellow dotted line). The data from spring season are marked as green right triangles, summer as red circles, autumn as yellow left triangles and winter as blue squares. The B–D) present probability density distribution of loss on ignition (*LOI*) in the following seasons: (B) spring, (C) summer, (D) autumn, and (E) winter. (For interpretation of the references to color in this figure legend, the reader is referred to the web version of this article.)

Table 1 The correlation coefficient R^2, number of measurements and robust linear regression for particulate inorganic matter (*PIM*) and particulate organic matter (*POM*) for different seasons.

	R^2	Number of measurements	Robust linear regression
Spring	0.56	135 during 5 days	$POM = 0.78 + 0.33 \cdot PIM$
Summer	0.08	212 during 4 days	No correlation
Autumn	0.59	93 during 2 days	$POM = 0.43 + 0.16 \cdot PIM$
Winter	0.59	30 during 2 days	Low number of measurements

In the ADCP surveys, the outflow from the eastern part of Hansbreen was the most evident, while the western and central outflows were only partly resolved (Fig. 4D–F, J–L). The values of *Int*, which reflect *SPM* concentration, were higher in July than in September. However, while both surveys showed that most of the *SPM* was contained to Hansbukta and that only a small amount escaped from the bay (Fig. 4C and I), the *SPM* distributions within the bay was different. In July, the *SPM* maximum was related to the major outflow from the eastern part of Hansbreen, while the two secondary maxima of *Int* were likely related to the outflow from the western part of Hansbreen and to the region in axial part of the bay, below 40 m deep, with rapid flow towards the glacier (Fig. 4D–F). In September, although the outlined maxima in *Int* were still visible, the *SPM* distribution was more uniform (Fig. 4L).

The *SPM* concentrations measured in the water samples ranged from 2.3 mg l^{-1} on the 24th of May 2016 at station H1_09 on the water surface to 82.8 mg l^{-1} on the 18th of June 2015 at station H5_05, which is close to main glacier outflow, at a 1 m depth. The mean *SPM* concentrations averaged for the daily data were the highest during the ablation season in the summer and early autumn, with a maximum average concentration in October 2015 (over 35 mg l^{-1}). The lowest average concentrations were measured during the winter and spring, and a minimum averaged concentration was documented in the 2015 spring season (below 10 mg l^{-1}) in a period shortly after the sea ice disappeared (Appendix A1,

Fig. 2E). The annual course of the changes in the *SPM* mean concentration is characterised by a rapid increase at the end of May and beginning of June 2015 (from 10 to more than 25 mg l^{-1}). After June, the mean concentration increased gradually until the end of October. The mean *SPM* concentration decreased during the late autumn and beginning of winter to approximately 25 mg l^{-1} in December. In April 2016, the mean *SPM* concentration was approximately 25 mg l^{-1} and increased to 35 mg l^{-1} in the second part of June. Moreover, an episodic increase of the *SPM* concentration was observed in the first half of May 2016 (Fig. 3E).

A comparison of the *SPM* distribution (Figs. 5–7) and mean *SPM* concentration in the surface waters (0–10 m) and deeper layers (below 20 m) (Fig. 3E) reveals clear seasonal variability. From June to September, the *SPM* was predominantly in the surface layer, while from November until May, it was predominantly in the deeper water. In October 2015, the amount of *SPM* in the surface waters was very similar to the amount in the deeper layers.

The *LOI* in the *SPM* ranged from 2.9% on the 9th of May 2016 at station H1_09 near the bottom of the bay to 70.6% on the same day at station H1_04 at a depth of 10 m. During the spring, the measured *LOI* mostly ranged between 20 and 40%, with a mode of approximately 25% (Fig. 8B). The highest average *LOI* (approximately 30%) was observed during the spring of 2016 (Appendix A2, Fig. 2F). During the summer season, the *LOI* achieved its lowest values and varied between 10 and 30% with a mode of approximately 15% (Fig. 8C). The values of *LOI* in the *SPM* during the autumn were similar to the values in the summer and ranged from 10 to 20% with a mode of approximately 15% (Fig. 8D). In the winter, the *LOI* in the *SPM* was slightly higher, ranging from 20 to 30% (Fig. 8E).

The highest concentrations of *POM* were measured during the spring and summer, and the highest concentrations of *PIM* were measured during the summer and autumn (Fig. 8A). No correlation was observed between the measured *POM* and *PIM* during the summer (R^2 = 0.08). During the winter, the correlation between *POM* and *PIM* was 0.59; however, there were too few measurements for linear regression to be calculated. The correlations between *POM* and *PIM* were 0.56 during the spring and 0.59 during the autumn (Table 1, Fig. 8A). The seasonal spatial variability of the *POM* and *PIM* distributions (Figs. 3F and 5–7) was similar to the total *SPM* concentration pattern.

5. Discussion

5.1. The studied seasons in the context of multiyear variability

During previous decades, due to specific oceanographic or meteorological conditions like the massive intrusion of AW into fjords, some years and seasons were exceptional (e.g. Cottier et al., 2005). However, the study period from 2015 to 2016 appears to be representative of typical conditions during the past decade when it is considered in a context of multiyear analyses of meteorological conditions from the PPS in Hornsund (Cisek et al., 2017; Osuch and Wawrzyniak, 2016, 2017), as well as snow coverage variability analyses (Kępski et al., 2017). A comparison of the study period to the general summer oceanographic condition in Hornsund also proved that the studied summer was similar to those observed in the previous years (Promińska et al., 2017). In the studied period, sea ice occurred in the spring of 2015 and was absent in 2016. However, as documented by Muckenhuber et al. (2016), the irregular presence of sea ice in Hornsund was also noticed during previous seasons. In terms of the range of the *SPM* concentrations, the measured summer values are similar to the concentrations that have been previously reported from tidewater glacier-affected bays in Svalbard, which usually have values ranging from a few to approximately 100 mg l^{-1} (Elverhøi et al., 1983; Görlich, 1986; Görlich et al., 1987; Svendsen et al., 2002; Szczuciński and Zajączkowski, 2012; Zajączkowski, 2008). Thus, the conditions during the studied period can be considered to be typical for contemporary subpolar fjords of Svalbard.

5.2. Sources of *SPM*

In Hansbukta, the *SPM* is mainly delivered through subglacial meltwater outflows from the cliff of Hansbreen. Based on satellite images (Fig. 1) and ADCP measurements (Fig. 4), we found that the positions of the outflows fluctuated during the studied period. However, the major subglacial meltwater discharge came from the eastern part of the ice cliff (Fig. 1), which was also predicted by a sub-glacial water flow model by Pälli et al. (2003). Hansbreen is a polythermal glacier (Jania et al., 1996); thus, meltwater discharge is possible throughout the year. However, the discharge becomes significant only during the ablation season (Fig. 2A), when the major glacial channels are unblocked due to the high pressure of the meltwater (Pälli et al., 2003). The available data does not allow for precise estimates of suspended sediment discharge. However, assuming that the documented near-surface *SPM*-rich brackish layer contains mainly sediment delivered from the outflows, a simple estimate can be made based on the July ADCP profile (Fig. 4D and E). Using the cross-sectional area of a *SPM*-rich surface water plume of approximately 2500 m^2, multiplying this value by a minimum southward flow velocity of 0.12 m s^{-1} and an average *SPM* concentration of 50 mg l^{-1}, the obtained minimum estimate of the sediment flux is in the order of 15 kg s^{-1}. If this value is multiplied by the three months of the effective ablation season that have relatively high discharge rates and divided by Hansbreen drainage basin area of approximately 55 km^2, it provides a sediment yield in order of 2000 t km^{-2} $year^{-1}$ (for the ablation season). This value is in the same order of magnitude as the sediment yields reported for subpolar and temperate glaciers (e.g., Gurnell et al., 1996; Koppes et al., 2015). Thus, it is very likely that the overwhelming majority of the *SPM* is delivered by the meltwater outflows and that the other *SPM* sources are secondary and may be important only seasonally.

Approximately one-fourth of the total ablation of Hansbreen is due to icebergs calving and ice front melting processes (Grabiec et al., 2012). The icebergs that are produced by Hansbreen are relatively small, and many of them are grounded and melted in the shallow parts of the Hansbukta (Ćwiąkała et al., 2018). Their contribution to the total *SPM* in the bay is relatively small. In the period from 2000 to 2008,

approximately 25.5 × 10^6 m^3 of ice was released as icebergs annually (Grabiec et al., 2012). Except in specific zones, such as 1–2 m thin basal ice layers or shear zones, the average percentage of debris in Hansbreen ranges from 0.05 to 0.5% (Rachlewicz and Szczuciński, 2000). Assuming an average rock density of approximately 2.5 kg m^{-3}, the annual sediment supply from melting icebergs is approximately 65; 5% of the daily supply from the meltwater outflows.

The remaining potential sources of *SPM* include transport by wind and surface runoff from the non-glaciated part of the Hansbukta drainage basin, coastal erosion, rafting by sea ice, biological production (e.g., phytoplankton blooms), import from the main fjord basin due to water exchange (e.g., due to tides) and the resuspension of previously deposited sediments. The supply of sediment from the non-glaciated land is negligible because it has a very small area and low relief. The majority of the terrestrial marginal zone of Hansbreen drains to adjacent bays (Fig. 1). In Hansbukta, no major coastal erosion is observed, although when the *SPM* concentrations from spring 2015 and 2016 are compared (Fig. 3D and E), they are higher in 2016, which is when no wave-protecting shore ice was observed.

The *POM* comes at least from two sources: supply of old organic matter from land and delivery of modern organic matter produced in marine environment. The recent works in Hornsund fjord applying carbon isotopes in organic matter in fjord sediments (Koziorowska et al., 2016; Szczuciński et al., 2017) and in *SPM* (Apolinarska et al., 2017) suggest that significant portion of organic carbon is delivered from erosion of older organic-rich sediments and rocks. This may also apply to the Hansbukta. However, the *POM* is at least partly derived from modern biological production, particularly in specific periods, for instance on the 9th of May 2016 (Fig. 5H) and on the 21st of December 2015 (Fig. 7H), when phytoplankton blooms and massive zooplankton advection likely occurred, respectively. Such phenomenons are commonly reported in the Arctic during the spring and autumn–winter seasons (e.g., Cowan et al., 1998; Görlich et al., 1987; Kwaśniewski et al., 2003; Rabindranath et al., 2008; Walkusz et al., 2003; Weydmann et al., 2013; Węsławski et al., 1988).

The *SPM* is also delivered by sediment resuspension from sill and shallow water regions. The resuspension is due to waves as well as water flow over the sill related to water exchange processes between Hansbukta and the main part of the Hornsund. The water exchange is driven by the tides, Coriolis-driven circulation patterns, as well as by water replacement due to freshwater supplies from meltwater outflows. This exchange of water is a typical oceanographic phenomenon in glacial bays separated by sills (e.g., Motyka et al., 2003; Rignot et al., 2010). The water exchange results in relatively fast near-bottom water flows (Fig. 4), in order of 15 cm s^{-1}, and sediment resuspension. The bottom of the bay around sill has relatively high *SPM* concentrations throughout the year (Figs. 5–7), which suggests that sediment resuspension from the sill is an important factor contributing to the *SPM* distribution in the bay.

5.3. Seasonality in *SPM* distribution

The seasonal changes in the *SPM* concentration, spatial distribution and composition (*POM*/*PIM*) result from the overlapping influences of a number of factors. The drivers discussed here include the duration of the ablation season, freshwater supply, glacial dynamics, *SPM* supply, water stratification and circulation in the bay, the bay bathymetry, presence of sea ice, light availability (polar day and night), biological productivity and sedimentary processes. Moreover, there are also several factors that were found important for *SPM* distribution in similar environments (Cowan and Powell, 1990; Gilbert et al., 2002; Görlich et al., 1987; Syvitski, 1989; Szczuciński and Zajączkowski, 2012) but cannot be here accurately evaluated due to the applied monthly sampling resolution. These factors include tides, storm events, daily fluctuations in the suspended sediment discharge and local wind damming effects.

5.3.1. Summer season

The summer distribution of *SPM*, with *SPM*-rich surface brackish water layer, is generally similar to the patterns that have been previously reported for tidewater glacier fronts (e.g., Curran et al., 2004; Görlich, 1986; Görlich et al., 1987; Syvitski, 1989; Szczuciński and Zajączkowski, 2012; Zajączkowski, 2002), although the 3D pictures provided by ADCP surveys (Fig. 4) showed the circulation to be more complex than previously believed. The intensive freshwater outflows that start in the spring-summer transition period (during June 2015 and May–June 2016) caused slight increase in the water temperature (Figs. 2C and 3A), a decrease in salinity (Fig. 2D and 3C) (transformation of WCW to LW), the development of water stratification (Fig. 3B), and increases in the *FWF* (Fig. 3D) and *SPM* concentration (Fig. 2E and 3E) in Hansbukta.

The large amount of *SPM* that was delivered to the bay was mainly confined to the approximately 10 m thick (Fig. 6) brackish surface water layer. Considering the total *SPM* supply, one could expect even higher *SPM* concentrations in the surface water; however, this water mass is in motion (Fig. 4A and B), and the *SPM* is partly exported from the bay by the surface currents. Moreover, *SPM* in surface layer is removed due to fast settling of flocculated particles.

The flocculation (aggregation) of *SPM*, documented by Laser In Situ Scattering and Transmissometry measurements (Szczuciński and Moskalik, 2017), is enhanced by high *SPM* concentrations, turbulence related to fast flow velocity and the mixing of saline water with freshwater. The *SPM* is composed of approximately 85% of grains smaller than 60 μm, as inferred from the bottom sediments (Görlich, 1986). However, the suspended aggregates that were observed during summer in the surface water layer had a mean floc grain size ranging from 30 to over 120 μm, and below the pycnocline were transferred only aggregates with a mean floc size over 125 μm, which is an equivalent of fine sand grain size fraction (Szczuciński and Moskalik, 2017).

Thus the well-developed pycnocline serves as a barrier for settling particles and is likely the major reason for the higher *SPM* concentrations in the surface water, in particular close to pycnocline (Figs. 3E and 6). During the summer, a steady increase in *FWF* (Fig. 3D) and a weakening of the stratification (Fig. 3B) reduced the role of pycnocline. Simultaneously faster increases in the *SPM* concentration in the deeper water was observed than in the nearby surface (Fig. 3E), which was possibly related to the longer residence time (slower settling rate) of smaller aggregates, which could settle through a smaller density gradient of the pycnocline.

The *SPM* concentration near the bottom of the bay (Fig. 6) is likely a result of resuspension due to the fast water flow over the sill separating Hansbukta from the main Hornsund basin, which was observed during the ADCP surveys (Fig. 4).

The *SPM* in the summer is mostly composed of *PIM*, while the *POM* concentration reaches a similar level to the *POM* concentration during the remaining part of the year. There is no correlation between the *POM* and *PIM* (Fig. 8A and C), which suggests various *SPM* sources or segregation processes. In the summer, *POM* is mainly concentrated along the lower boundary of the surface brackish layer (Fig. 6). According to a commonly reported model (e.g., Lydersen et al., 2014), the *POM* maximum is likely related to zooplankton, which is pumped to Hansbukta at depth with fjord water in exchange for the exported brackish surface water. The fjord waters upwell next to the ice front and the zooplankton population experiences massive mortality rates due to osmotic shock (Węsławski and Legeżyńska, 1998; Zajączkowski and Legeżyńska, 2001). Consequently, such settings are well-known feeding grounds for birds and mammals (Lydersen et al., 2014; Urbanski et al., 2017).

5.3.2. Autumn season

The annual maximum mean *SPM* concentration occurred in the middle of the autumn season (Fig. 3E). During that time, the *SPM*, *POM* and *PIM* distributions were relatively uniform (Fig. 7) in the surface and deeper water masses (Fig. 3E and F). This is likely due to several processes: the density-driven vertical mixing of water in the bay and disappearance of the water stratification (Fig. 3B), enhanced resuspension and mixing during frequent in autumn storms (Wojtysiak et al., 2018), and a reduction in flocculation processes that elongates the residence time of the *SPM* in the water column. The latter was reported also for autumn season in the glacial bay of Adolfbukta (central Spitsbergen) by Szczuciński and Zajączkowski (2012). They compared the summer and autumn conditions and found that the vertical particulate matter fluxes measured with sediment traps decreased by an order of magnitude in the autumn, while the *SPM* concentrations decreased only two-fold. Szczuciński and Zajączkowski (2012) interpreted these observations as a result of a decrease in *SPM* flocculation, resulting in the slowing of the settling rate and the elongation of *SPM* residence times in the water column. However, in contrary to their study, in Hansbukta the *SPM* concentration increased in the autumn. The major reason for the difference may be the fact that Adolfbukta lacks a shallow sill, thus *SPM* may be easily exported from the bay and potential sediment resuspension is limited. In Hansbukta, the presence of a shallow sill causes the *SPM* to be trapped in the bay and enriched in resuspended sediment due to accelerated water flow over the sill.

In November, the *SPM* concentration decreased, particularly in the surface water layer (Figs. 3E and 7A, D), which was depleted of *SPM* due to successive *SPM* settling that was not compensated by the delivery of new *SPM*.

POM and *PIM* concentrations are correlated in autumn (Table 1, Fig. 8A and D). The correlation is likely due to efficient mixing of the *SPM* during the autumn. In December and at the end of autumn (Fig. 7H), an increase in the *POM* concentration in the subsurface waters of the central part of the bay was observed. At that time, the supply from the land had already ceased, air temperatures were well below 0°C, and the primary production in the water was at its lowest level due to the polar night conditions, so the most likely source of the elevated *POM* was the advection of rich in zooplankton fjord and/or shelf waters, as was mentioned in other studies (e.g.: Rabindranath et al., 2008; Walkusz et al., 2009; Weydmann et al., 2013; Węsławski et al., 1988; Zajączkowski et al., 2010).

5.3.3. Winter season

During the winter, the mean *SPM* concentrations reached minimum values in the surface layer, but the water column average remained same as during the summer season (Fig. 3E). The *SPM* was mainly concentrated in the deeper part of the bay (Fig. 7G and J), particularly above the sill, on the sill slope and near the glacier. This may suggest that a major source of *SPM* is the resuspension of sediments, particularly in shallow areas. In the winter, the *SPM* largely comes from the recycling of previously delivered material. The partial exposure of the bay to oceanic swell, the tidal currents and the relatively shallow sill that confines the bay and accelerates flow may all contribute to resuspension of sediments and sustain the *SPM* in suspension. Since Hansbreen is a polythermal glacier (Jania et al., 1996), it is also possible that there are some minor subglacial discharges of suspended sediment in winter.

5.3.4. Spring season

The studied period encompassed two spring seasons, which differed in terms of sea ice conditions. During the spring of 2016, which had no sea ice cover, the average *SPM*, *POM* and *PIM* concentrations were similar to the concentrations of the previous autumn and winter seasons (Figs. 2E and 3E, F). The spatial *SPM* distribution was also the same as the distribution in the winter before the onset of ablation (April) and developed into the summer distribution by an increase in the surface water layer in the weeks following the ablation onset (Fig. 6D–O). The conditions were different in spring 2015, when sea ice cover and well-developed shore ice occurred (Figs. 2, 3 and 6) and the *SPM*, *POM* and *PIM* were the lowest. In both of the spring seasons, the *PIM* and *POM* were correlated (Table 1, Fig. 8A and B), which may suggest that the *SPM* is largely composed of the same material, which is reworked over time. The difference between the 2015 and 2016 spring seasons is likely mainly due to sea ice occurrence during 2015 and limited wave action during this season.

Although *POM* and *PIM* generally correlate, there were also some differences. This was most likely a result of a phytoplankton bloom increasing suspended *POM* concentrations, as commonly occur in the Arctic during the spring season (e.g., Cowan et al., 1998; Görlich et al., 1987; Pawłowska et al., 2011; Węsławski et al., 1988; Zajączkowski et al., 2010). Such situation was documented on the 9th of May 2016 (Fig. 5H).

5.4. Implications for remote sensing based studies

The estimates of freshwater and *SPM* delivery to the coastal ocean from tidewater glaciers and the assessment of their global importance require the application of remote sensing methods that allow simultaneous measurements over large

areas. While these methods appeared to be successful in estimating the sediment supplies of meltwater rivers (e.g., Overeem et al., 2017), they are still of limited use in the case of fjords. The in situ investigations of *SPM* deliveries and distributions near tidewater glacier fronts are often dangerous, expensive and time-consuming, so investigations applying analyses of satellite images are particularly useful (e.g., Hodgkins et al., 2016; Hudson et al., 2014; Schildt et al., 2017; Urbanski et al., 2017). However, they have a number of restrictions. For example, they are usually limited to the short summer season, they must be calibrated with in situ data and they only provide information about surface water. It is commonly assumed that the major *SPM* discharge near tidewater glacier fronts is limited to the brackish surface layer of the water in front of tidewater glaciers. However, the present study shows that a maximum amount of the *SPM* during the summer is at the lower boundary of the surface brackish water layer, which is approximately 10 m thick. Moreover, during the majority of the year, most of the *SPM* is located in deeper waters (>20 m), which is also the case during the period with maximum average *SPM* concentrations in early autumn (Fig. 3E). Thus, the remote sensing data must be carefully interpreted when water surface reflectance is used to estimate the *SPM* concentration because subsurface *SPM* concentrations may be even higher than at the surface.

6. Conclusions

The study presents the first monitoring data of *SPM* concentrations in a sub-polar glacial bay in context of its local oceanographic and meteorological conditions over almost one year. The observed seasonal *SPM* concentration variations appear to result not only from the dominant glacial meltwater input that delivers the vast majority of *SPM* but also from the intensity of flocculation processes that control the residence period of the particles in the water, the resuspension of *SPM* and biological productivity. The documented circulation pattern appears to be more complex than the patterns typically assumed in simple 2D models and is strongly affected by the presence of shallow sill at the entrance. In Hansbukta, the highest single *SPM* concentration value was measured at the beginning of the summer, but the mean *SPM* value gradually increased during the summer with a peak in the autumn, long after the freshwater discharge maximum. During the summer, the *SPM* was mainly concentrated in the surface water layer; during the rest of the year, the opposite occurred, with higher *SPM* levels observed in the deep water layer. Generally, the *POM* content of the *SPM* was stable, except during spring phytoplankton blooms (maximum *POM* concentration) and spring periods with sea ice cover (minimum *POM* concentration).

Author contributions

Mateusz Moskalik and Witold Szczuciński wrote the final version of the manuscript. Mateusz Moskalik made all the data calculations and analyses, prepared the material for the figures and led the discussions. Joanna Ćwiąkała participated in laboratory work and partly wrote the manuscript. Aleksander Dominiczak participated in laboratory work. All authors helped prepare the discussion and conclusion sections.

Acknowledgements

This publication was financed by the statutory activities No 3841/E-41/S/2016 of the Ministry of Science and Higher Education of Poland and by the funds of the Leading National Research Centre (KNOW), received by the Centre for Polar Studies, for the period 2014—2018. W.S., A.D., P.Z. and partly M.M. were supported by the Polish National Science Centre (NCN) grant No. 2013/10/E/ST10/00166.

We thank the Institute of Geophysics PAS (especially Tomasz Wawrzyniak, Maciej Błaszkowski, Mariusz Czarnul) for providing meteorological and oceanographical data used in this investigation and the Polish Polar Station Hornsund staff for establishing and maintaining the meteorological site and oceanographical monitoring. We also thank Urszula Hordyjewska-Cejko and Kamila Jarosz from Marie Curie Skłodowska University in Lublin and Paweł Kaczmarek from Adam Mickiewicz University in Poznań for their help with laboratory work. Constructive comments by two anonymous reviewers and the editor — Prof. Janusz Pempkowiak, contributed to the improvement of the manuscript and are gratefully acknowledged.

Appendix A. Supplementary data

Supplementary data associated with this article can be found, in the online version, at doi:10.1016/j.oceano.2018.03.001.

References

Apolinarska, K., Szczuciński, W., Moskalik, M., Dominiczak, A., 2017. Seasonal changes, spatial variability and origin of suspended organic matter in Hornsund, Spitsbergen. EGU General Assembly 2017. Geophys. Res. Abstracts 19, EGU2017-10283.

Bennett, M., Glasser, N., 2009. Glacial Geology: Ice Sheets and Landforms. Wiley Blackwell, 385 pp.

Bhatia, M.P., Kujawinski, E.B., Das, S.B., Breier, C.F., Henderson, P. B., Charette, M.A., 2013. Greenland meltwater as a significant and potentially bioavailable source of iron to the ocean. Nat. Geosci. 6, 274—278, http://dx.doi.org/10.1038/ngeo1746.

Birkenmajer, K., 1990. Geology of Hornsund Area, Spitsbergen. Map 1:75000 and Explanations. Silesia Univ, Katowice.

Błaszczyk, M., Jania, J., Hagen, J.O., 2009. Tidewater glaciers of Svalbard: recent changes and estimates of calving fluxes. Polish Polar Res. 30 (2), 85—142.

Błaszczyk, M., Jania, J.A., Kolondra, L., 2013. Fluctuations of tidewater glaciers in Hornsund Fjord (Southern Svalbard) since the beginning of the 20th century. Polish Polar Res. 34 (4), 327—352, http://dx.doi.org/10.2478/popore-2013-0024.

Boldt, K.V., Nittrouer, C.A., Hallet, B., Koppes, M.N., Forrest, B.K., Wellner, J.S., Anderson, J.B., 2013. Modern rates of glacial sediment accumulation along a 15° S-N transect in fjords from the Antarctic Peninsula to southern Chile. J. Geophys. Res.-Earth 118, 2072—2088, http://dx.doi.org/10.1002/jgrf.20145.

Carr, R., Stokes, C.R., Vieli, A., 2017. Threefold increase in marine-terminating outlet glacier retreat rates across the Atlantic Arctic: 1992—2010. Ann. Glaciol. 58 (74), 72—91, http://dx.doi.org/10.1017/aog.2017.3.

Chauche, N., Hubbard, A., Gascard, J.C., Box, J.E., Bates, R., Koppes, M., Sole, A., Patton, H., 2014. Ice-ocean interaction and calving front morphology at two west Greenland tidewater

outlet glaciers. Cryosphere 8, 1457—1468, http://dx.doi.org/10.5194/tc-8-1457-2014.

Cisek, M., Makuch, P., Petelski, T., 2017. Comparison of meteorological conditions in Svalbard fjords: Hornsund and Kongsfjorden. Oceanologia 59 (4), 413—421, http://dx.doi.org/10.1016/j.oceano.2017.06.004.

Cottier, F.R., Tverberg, V., Inall, M.E., Svendsen, H., Nilsen, F., Griffiths, C., 2005. Water mass modification in an Arctic fjord through cross-shelf exchange: the seasonal hydrography of Kongsfjorden, Svalbard. J. Geophys. Res. 110, C12005, http://dx.doi.org/10.1029/2004JC002757.

Cowan, E.A., Cai, J., Powell, R.D., Seramur, K.C., Spurgeon, V.L., 1998. Modern tidal rhythmites deposited in a deep-water estuary. Geo-Mar. Lett. 18 (1), 40—48, http://dx.doi.org/10.1007/s003670050.

Cowan, E., Powell, R.D., 1990. Suspended sediment transport and deposition of cyclically interlaminated sediment in a temperate glacial fjord, Alaska, U.S.A. In: Dowdeswell, J.A., Scourse, J.D. (Eds.), Glacimarine Environments: Processes and Sediments. Geol. Soc. Spec. Publ. 53, 75—89.

Curran, K.J., Hill, P.S., Milligan, T.G., Cowan, E.A., Syvitski, J.P.M., Konings, S.M., 2004. Fine-grained sediment flocculation below the Hubbard Glacier meltwater plume, Disenchantment Bay, Alaska. Mar. Geol. 203, 83—94, http://dx.doi.org/10.1016/S0025-3227(03)00327-X.

Ćwiąkała, J., Moskalik, M., Forwick, M., Wojtysiak, K., Giżejewski, J., Szczuciński, W., 2018. Submarine geomorphology at the front of the retreating Hansbreen tidewater glacier Hansbreen, Hornsund fjord, southwest Spitsbergen. J. Maps 14 (2), 123—134, http://dx.doi.org/10.1080/17445647.2018.1441757.

Deines, K.L., 1999. Backscatter estimation using Broadband acoustic Doppler current profilers. In: Anderson, S.P., Terray, E.A., Rizoli White, J.A., Williams, A.J. (Eds.), Proceedings of the IEEE Sixth Working Conference on Current Measurement, San Diego, CA, 249—253.

Dowdeswell, J.A., Cromack, C., 1991. Behavior of a glacier-derived suspended sediment plume in a small Arctic inlet. J. Geol. 99, 111—123, http://dx.doi.org/10.1086/629477.

Dowdeswell, J.A., Hogan, K.A., Arnold, N.S., Mugford, R.I., Wells, M. J., Hirst, P.P., Decalf, C., 2015. Sediment-rich meltwater plumes and ice-proximal fans at the margins of modern and ancient tidewater glaciers: observations and modelling. Sedimentology 62 (6), 1665—1692, http://dx.doi.org/10.1111/sed.12198.

Drewnik, A., Węsławski, J.M., Włodarska-Kowalczuk, M., Łącka, M., Promińska, A., Zaborska, A., Gluchowska, M., 2016. From the worm's point of view. I: Environmental settings of benthic ecosystems in Arctic fjord (Hornsund, Spitsbergen). Polar Biol. 39 (8), 1411—1424, http://dx.doi.org/10.1007/s00300-015-1867-9.

Elverhøi, A., Lønne, Ø., Seland, R., 1983. Glaciomarine sedimentation in a modern fjord environment, Spitsbergen. Polar Res. 1 (2), 127—149, http://dx.doi.org/10.1111/j.1751-8369.1983.tb00697.x.

Forwick, M., Vorren, T.O., Hald, M., Korsun, S., Roh, Y., Vogt, C., Yoo, K.-C., 2010. Spatial and temporal influence of glaciers and rivers on the sedimentary environment in Sassenfjorden and Tempelfjorden, Spitsbergen. In: Howe, J.A., Austin, W.E.N., Forwick, M., Paetzel, M. (Eds.), Fjords Systems and Archives, vol. 344. Geological Soc., Spec. Publ., London, 165—195, http://dx.doi.org/10.1144/SP344.13.

Gilbert, R., Nielsen, N., Möller, H., Desloges, J.R., Rasch, M., 2002. Glaciomarine sedimentation in Kangerdluk (Disko Fjord), West Greenland, in response to a surging glacier. Mar. Geol. 191, 1—18, http://dx.doi.org/10.1029/2002GC000441.

Görlich, K., 1986. Glacimarine sedimentation of muds in Hornsund Fjord, Spitsbergen. Ann. Soc. Geol. Pol. 56, 433—477.

Görlich, K., Węsławski, J.M., Zajączkowski, M., 1987. Suspension settling effect on macrobenthos biomass distribution in the Hornsund fjord, Spitsbergen. Polish Polar Res. 5, 175—192, http://dx.doi.org/10.1111/j.1751-8369.1987.tb00621.x.

Grabiec, M., Jania, J., Puczko, D., Kolondra, L., Budzik, T., 2012. Surface and bed morphology of Hansbreen, a tidewater glacier in Spitsbergen. Polish Polar Res. 33 (2), 111—138, http://dx.doi.org/10.2478/v10183-012-0010-7.

Gurnell, A., Hannah, D., Lawler, D., 1996. Suspended sediment yield from glacier basins. In: Erosion and Sediment Yield: Global and Regional Perspectives. IAHS Publ. 236, 97—104.

Heiri, O., Lotter, A.F., Lemcke, G., 2001. Loss on ignition as a method for estimating organic and carbonate content in sediments: reproducibility and comparability of results. J. Paleolimmnol. 25, 101—110, http://dx.doi.org/10.1023/A:100811961.

Hodgkins, R., Bryant, R., Darlington, E., Brandon, M., 2016. Pre-melt-season sediment plume variability at Jökulsárlón, Iceland, a preliminary evaluation using in-situ spectroradiometry and satellite imagery. Ann. Glaciol. 57 (73), 39—46, http://dx.doi.org/10.1017/aog.2016.20.

Hudson, B., Overeem, I., McGrath, D., Syvitski, J.P.M., Mikkelsen, A., Hasholt, B., 2014. MODIS observed increase in duration and spatial extent of sediment plumes in Greenland fjords. Cryosphere 8, 1161—1176, http://dx.doi.org/10.5194/tc-8-1161-2014.

Jakacki, J., Przyborska, A., Kosecki, S., Sundfjord, A., Albretsen, J., 2017. Modeling of the Svalbard Fjord Hornsund. Oceanologia 59 (4), 473—495, http://dx.doi.org/10.1016/j.oceano.2017.04.004.

Jania, J., Mochnacki, D., Gądek, B., 1996. The thermal structure of Hansbreen, a tidewater glacier in southern Spitsbergen, Svalbard. Polar Res. 15, 53—66.

Ketchum, B.H., 1950. Hydrographic factors involved in the dispersion of pollutants introduced into tidal waters. J. Boston Soc. Civ. Eng. 37, 296—314.

Kępski, D., Luks, B., Migała, K., Wawrzyniak, T., Westermann, S., Wojtuń, B., 2017. Terrestrial remote sensing of snowmelt in a diverse High-Arctic tundra environment using time-lapse imagery. Remote Sens. 9 (7), 733, http://dx.doi.org/10.3390/rs9070733.

Kim, Y.H., Voulgaris, G., 2003. Estimation of suspended sediment concentration in estuarine environments using acoustic backscatter from an ADCP. In: Davis, R.A., Sallenger, A., Howd, P. (Eds.), Proc. International Conference on Coastal Sediments, Sheraton Sand Key Resort, 18—23 May 2003, Clearwater Beach, FL, USA.

Koppes, M.N., Hallet, B., 2002. Influence of rapid glacial retreat on the rate of erosion by tidewater glaciers. Geology 30 (1), 47—50, http://dx.doi.org/10.1130/0091-7613(2002)030<0047:IORGRO>2.0.CO;2.

Koppes, M., Hallet, B., Rignot, E., Mouginot, J., Wellner, J.S., Boldt, K., 2015. Observed latitudinal variations in erosion as a function of glacier dynamics. Nature 526, 100—103, http://dx.doi.org/10.1038/nature15385.

Koziorowska, K., Kuliński, K., Pempkowiak, J., 2016. Sedimentary organic matter in two Spitsbergen fjords: terrestrial and marine contributions based on carbon and nitrogen contents and stable isotopes composition. Cont. Shelf Res. 113, 38—46, http://dx.doi.org/10.1016/j.csr.2015.11.010.

Kwaśniewski, S., Hop, H., Falk-Petersen, S., Pedersen, G., 2003. Distribution of Calanus species in Kongsfjorden, a glacial fjord in Svalbard. J. Plankton Res. 25 (1), 1—20, http://dx.doi.org/10.1093/plankt/25.1.1.

Lydersen, C., Assmy, P., Falk-Petersen, S., Kohler, J., Kovacs, K.M., Reigstad, M., Steen, H., Strøm, H., Sundfjord, A., Varpe, Ø., Walczowski, W., Weslawski, J.M., Zajaczkowski, M., 2014. The importance of tidewater glaciers for marine mammals and seabirds in Svalbard, Norway. J. Mar. Sys. 129, 452—471, http://dx.doi.org/10.1016/j.jmarsys.2013.09.006.

Łupikasza, E., 2013. Atmospheric precipitation. In: Marsz, A.A., Styszyńska, A. (Eds.), Climate and Climate Change at Hornsund, Svalbard. Gdynia Maritime Univ., Gdynia, 402 pp.

Markussen, T.N., Elberling, B., Winter, C., Andersen, T.J., 2016. Flocculated meltwater particles control Arctic land-sea fluxes

of labile iron. Sci. Rep. 6, 24033, http://dx.doi.org/10.1038/srep24033.

Marsz, A.A., Styszyńska, A., 2013. Climate and Climate Change at Hornsund, Svalbard. Gdynia Maritime Univ., Gdynia, 402 pp.

Molnia, B.F., 2007. Late nineteenth to early twenty-first century behavior of Alaskan glaciers as indicators of changing regional climate. Global Planet. Change 56, 23—56, http://dx.doi.org/10.1016/j.gloplacha.2006.07.011.

Motyka, R.J., Hunter, L., Echelmeyer, K.A., Connor, C., 2003. Submarine melting at the terminus of a temperate tidewater glacier, LeConte Glacier, Alaska, U.S.A. Ann. Glaciol. 36, 57—65, http://dx.doi.org/10.3189/172756403781816374.

Muckenhuber, S., Nilsen, F., Korosov, A., Sandven, S., 2016. Sea ice cover in Isfjorden and Hornsund, Svalbard (2000—2014) from remote sensing data. Cryosphere 10 (1), 149—158, http://dx.doi.org/10.5194/tc-10-149-2016.

Nilsen, F., Cottier, F., Skogseth, R., Mattsson, S., 2008. Fjord-shelf exchanges controlled by ice and brine production: the interannual variation of Atlantic Water in Isfjorden, Svalbard. Cont. Shelf Res. 28, 1838—1853, http://dx.doi.org/10.1016/j.csr.2008.04.015.

Nut, D.C., Coachman, L.K., 1956. The oceanography of Hebron Fjord, Labrador. J. Fish. Res. Board. Can. 13 (5), 709—758, http://dx.doi.org/10.1139/f56-043.

Osuch, M., Wawrzyniak, T., 2016. Inter- and intra-annual changes in air temperature and precipitation in western Spitsbergen. Int. J. Climatol. 37 (7), 3082—3097, http://dx.doi.org/10.1002/joc.4901.

Osuch, M., Wawrzyniak, T., 2017. Variations and changes in snow depth at meteorological stations Barentsburg and Hornsund (Spitsbergen). Ann. Glaciol. 58 (75 pt 1), 11—20, http://dx.doi.org/10.1017/aog.2017.20.

Overeem, I., Hudson, B.D., Syvitski, J.P.M., Mikkelsen, A.B., Hasholt, B., van den Broeke, M.R., Noël, B.P.Y., Morlighem, M., 2017. Substantial export of suspended sediment to the global oceans from glacial erosion in Greenland. Nat. Geosci. 10, 859—863, http://dx.doi.org/10.1038/ngeo3046.

Pawłowska, J., Włodarska-Kowalczuk, M., Zajączkowski, M., Nygård, H., Berge, J., 2011. Seasonal variability of meio- and macrobenthic standing stocks and diversity in an Arctic fjord (Adventfjorden, Spitsbergen). Polar Biol. 34, 833—845, http://dx.doi.org/10.1007/s00300-010-0940-7.

Pawłowska, J., Zajączkowski, M., Szczuciński, W., Zaborska, A., Kucharska, M., Jernas, P.E., Forwick, M., 2017. The influence of Coriolis force driven water circulation on the palaeoenvironment of Hornsund (S Spitsbergen) over the last century. Boreas 46 (4), 737—749, http://dx.doi.org/10.1111/bor.12249.

Pälli, A., Moore, J.C., Jania, J., Kolondra, L., Głowacki, P., 2003. The drainage pattern of Hansbreen and Werenskioldbreen, two polythermal glaciers on Svalbard. Polar Res. 22 (2), 355—371, http://dx.doi.org/10.1111/j.1751-8369.2003.tb00117.x.

Promińska, A., Cisek, M., Walczowski, W., 2017. Kongsfjorden and Hornsund hydrography — comparative study based on a multiyear survey in fjords of west Spitsbergen. Oceanologia 59 (4), 397—412, http://dx.doi.org/10.1016/j.oceano.2017.07.003.

Rabindranath, A., Daase, M., Falk-Peteresen, S., Wold, A., Wallace, M.I., Berge, J., Brierley, A.S., 2008. Seasonal and diel vertical migration of zooplankton in the High Arctic during the autumn midnight sun of 2008. Mar. Biodivers. 41 (3), 365—382, http://dx.doi.org/10.1007/s12526-010-0067-7.

Rachlewicz, G., Szczuciński, W., 2000. Ice tectonics and bedrock relief control on glacial sedimentation — an example from Hansbreen, Spitsbergen. In: Polish Polar Studies. 27th Polar Symposium. 259—275.

Radić, V., Hock, R., 2011. Regionally differentiated contribution of mountain glaciers and ice caps to future sea-level rise. Nat. Geosci. 4, 91—94, http://dx.doi.org/10.1038/ngeo1052.

Rignot, E., Koppes, M., Velicogna, I., 2010. Rapid submarine melting of the calving faces of West Greenland glaciers. Nat. Geosci. 3, 187—191, http://dx.doi.org/10.1038/ngeo765.

Sagan, S., Darecki, M., 2018. Inherent optical properties and particulate matter distribution in summer season in waters of Hornsund and Kongsfjordenen, Spitsbergen. Oceanologia 60 (1), 65—75, http://dx.doi.org/10.1016/j.oceano.2017.07.006.

Schildt, K.M., Hawley, R.L., Chipman, J.W., Benn, D.I., 2017. Quantifying suspended sediment concentration in subglacial sediment plumes discharging from two Svalbard tidewater glaciers using Landsat-8 and in-situ measurements. Int. J. Remote Sens. 38, 6865—6881, http://dx.doi.org/10.1080/01431161.2017.1365388.

Solomina, O.N., Bradley, R.S., Jomelli, V., Geirsdottir, A., Kaufman, D.S., Koch, J., McKay, N.P., Masiokas, M., Miller, G., Nesje, A., Nicolussi, K., Owen, L.A., Putnam, A.E., Wanner, H., Wiles, G., Yang, B., 2016. Glacier fluctuations during the past 2000 years. Quat. Sci. Rev. 149, 61—90, http://dx.doi.org/10.1016/j.quascirev.2016.04.008.

Straneo, F., Heimbach, P., 2013. North Atlantic warming and the retreat of Greenland's outlet glaciers. Nature 504, 36—43, http://dx.doi.org/10.1038/nature12854.

Svendsen, H., Beszczynska-Møller, A., Lefauconnier, B., Tverberg, V., Gerland, S., Jon Børre Ørbæk, J., Bischof, K., Pappuci, C., Zajączkowski, M., Azzolini, R., Bruland, O., Wiencke, Ch., Winther, J.G., Dallmann, W., 2002. The physical environment of Kongsfjorden-Krossfjorden, an Arctic fjord system in Svalbard. Polar Res. 21 (1), 133—166, http://dx.doi.org/10.1111/j.1751-8369.2002.tb00072.x.

Syvitski, J.P.M., 1989. On the deposition of sediment within glacier-influenced fjords: oceanographic controls. Mar. Geol. 85, 301—329, http://dx.doi.org/10.1016/0025-3227(89)90158-8.

Szczuciński, W., Dominiczak, A., Apolinarska, K., Forwick, M., Goslar, T., Moskalik, M., Strzelecki, M., Woszczyk, M., 2017. Climate-driven variations in source-to-sink fluxes of sediment and carbon in High Arctic fjord (Hornsund, Svalbard). In: 33rd International Meeting of Sedimentology and 16ème Congrés Français Sédimentologie, Toulouse. 10—12 October 2017 Abstract Book, 863.

Szczuciński, W., Moskalik, M., 2017. Sediment flocculation in fjords: tidewater glacier bay vs river-dominated bay. In: 33rd International Meeting of Sedimentology and 16ème Congrés Français Sédimentologie, Toulouse. 10—12 October 2017 Abstract Book, 864.

Szczuciński, W., Zajączkowski, M., Scholten, J., 2009. Sediment accumulation rates in subpolar fjords — impact of post-Little Ice Age glaciers retreat, Billefjorden, Svalbard. Estuar. Coast. Shelf Sci. 83 (3), 345—356, http://dx.doi.org/10.1016/j.ecss.2009.08.021.

Szczuciński, W., Zajączkowski, M., 2012. Factors controlling downward fluxes of particulate matter in glacier-contact and non-glacier contact settings in a subpolar fjord (Billefjorden, Svalbard). In: Li, M., Sherwood, C., Hill, P. (Eds.), Sediments, Morphology and Sedimentary Processes on Continental Shelves. IAS Spec. Publ., vol. 44. Wiley-Blackwell Publ., 369—385, http://dx.doi.org/10.1002/9781118311172.ch18.

Trusel, L.D., Powell, R.D., Cumpston, R.M., Brigham-Grette, J., 2010. Modern glaciomarine processes and potential future behaviour of Kronebreen and Kongsvegen polythermal tidewater glaciers, Kongsfjorden, Svalbard. In: Howe, J.A., Austin, W.E.N., Forwick, M., Paetzel, M. (Eds.), Fjord Systems and Archives, vol. 344. Geological Soc., Spec. Publ., London, 89—102, http://dx.doi.org/10.1144/SP344.9.

Urbanski, J.A., Stempniewicz, L., Węsławski, J.M., Dragańska-Deja, K., Wochna, A., Goc, M., Iliszko, L., 2017. Subglacial discharges create fluctuating foraging hotspots for sea birds in tidewater glacier bays. Sci. Rep. 7, 43999, http://dx.doi.org/10.1038/srep43999.

Walkusz, W., Storemark, K., Skau, T., Gannefors, C., Lundberg, M., 2003. Zooplankton community structure; a comparison of the fjords, open water and ice stations in the Svalbard area. Polish Polar Res. 24, 149—165.

Walkusz, W., Kwaśniewski, S., Falk-Petersen, S., Hop, H., Tverberg, V., Wieczorek, P., Weslawski, J.M., 2009. Seasonal and spatial changes in the zooplankton community of Kongsfjorden, Svalbard. Polar Res. 28, 254—281, http://dx.doi.org/10.1111/j.1751-8369.2009.00107.x.

Weydmann, A., Søreide, J.E., Kwaśniewski, S., Leu, E., Falk-Petersen, S., Berge, J., 2013. Ice-related seasonality in zooplankton community composition in a high Arctic fjord. J. Plankton Res. 35 (4), 831—842, http://dx.doi.org/10.1093/plankt/fbt031.

Węsławski, J.M., Legeżyńska, J., 1998. Glacier induced zooplankton mortality? J. Plankton Res. 20, 1233—1240.

Węsławski, J.M., Jankowski, A., Kwaśniewski, S., Swerpel, S., Ryg, M., 1991. Summer hydrology and zooplankton in two Spitsbergen fjords. Polish Polar Res. 12, 445—460.

Węsławski, J.M., Koszteyn, J., Zajaczkowski, M., Wiktor, J., Kwaśniewski, S., 1995. Fresh water in Svalbard fjord ecosystems. In: Skjodal, H.R., Hopking, C., Erikstad, K.E., Leinaa, H.P. (Eds.), Ecology of Fjords and Coastal Waters. Elsevier, Amsterdam, 229—241.

Węsławski, J.M., Zajączkowski, M., Kwaśniewski, S., Jezierski, J., Moskal, W., 1988. Seasonality in an Arctic fjord ecosystem: Hornsund, Spitsbergen. Polar Res. 6, 185—189.

Winters, G.V., Syvitski, J.P.M., 1992. Suspended sediment character and distribution in McBeth Fiord, Baffin Island. Arctic 45 (1), 25—35.

Wojtysiak, K., Herman, A., Moskalik, M., 2018. Wind wave climate of west Spitsbergen: seasonal variability and extreme events. Oceanologia, http://dx.doi.org/10.1016/j.oceano.2018.01.002.

Zajączkowski, M., Legeżyńska, J., 2001. Estimation of zooplankton mortality caused by an Arctic glacier outflow. Oceanologia 43 (3), 341—351.

Zajączkowski, M., Nygård, H., Hegseth, E.N., Berge, J., 2010. Vertical flux of particulate matter in an Arctic fjord: the case of lack of the sea-ice cover in Adventfjorden 2006—2007. Polar Biol. 33, 223—239, http://dx.doi.org/10.1007/s00300-009-0699-x.

Zajączkowski, M., Szczuciński, W., Bojanowski, R., 2004. Recent changes in sediment accumulation rates in Adventfjorden, Svalbard. Oceanologia 46 (2), 217—231.

Zajączkowski, M., Włodarska-Kowalczuk, M., 2007. Dynamic sedimentary environments of Arctic glacier-fed river estuary (Adventfjorden, Svalbard). I. Flux, deposition, and sediment dynamics. Estuar. Coast. Shelf Sci. 74, 285—296, http://dx.doi.org/10.1016/j.ecss.2007.04.015.

Zajączkowski, M., 2002. On the use of sediment traps in sedimentation measurements in glaciated fjords. Polish Polar Res. 23, 161—174.

Zajączkowski, M., 2008. Sediment supply and fluxes in glacial and outwash fjords, Kongsfjorden and Adventfjorden, Svalbard. Polish Polar Res. 29 (1), 59—72.